Acta Oceanol. Sin., 2024, Vol. 43, No. 11, P. 68–87
https://doi.org/10.1007/s13131-024-2380-1
http://www.aosocean.com
E-mail: ocean2@hyxb.org.cn

Spatiotemporal variations of phytoplankton in the Taiwan Strait using lipid biomarkers and the potential influencing factors

Zitong Liu[1, 2], Shuqin Tao[2, 3*], Xiang Ye[2, 3], Aijun Wang[2, 3, 4], Chang Ran[2], Shuilan Wu[2], Zhen Jiang[2], Junwen Wu[1*]

[1] Guangdong Provincial Key Laboratory of Marine Disaster Prediction and Prevention/Institute of Marine Sciences, Shantou University, Shantou 515063, China

[2] Third Institute of Oceanography, Ministry of Natural Resources, Xiamen 361005, China

[3] Fujian Provincial Key Laboratory of Marine Physical and Geological Processes, Xiamen 361005, China

[4] Observation and Research Station of Island of Coastal Ecosystem in the Western Taiwan Strait, Ministry of Natural Resources, Xiamen 361005, China

Received 30 December 2023; accepted 31 May 2024

Abstract

The biological pump, driven by phytoplankton production and death, plays a crucial role in the ocean's sequestration of atmospheric CO_2. In particular, marginal seas with high primary productivity show a significant capacity for carbon fixation. Variations in phytoplankton biomass and community structure are key factors influencing the efficiency of the marine biological pump. The Taiwan Strait (TS) is a unique shallow conduit that connects the East China Sea (ECS) and the South China Sea (SCS), which are subject to seasonal monsoons and episodic events (e.g., typhoons and floods). Thus, its planktonic ecosystem is significantly influenced by physical processes such as strong ocean currents, coastal upwelling and river discharge, resulting in noticeable seasonal variability. In this study, we examined spatiotemporal patterns of phytoplankton biomass and community structure using phytoplankton-sourced biomarkers from suspended particles in surface waters across all four seasons from 2019 to 2020 in the TS. The findings highlight notable seasonal disparities in phytoplankton biomass, with spring and summer exhibiting significantly higher levels compared to autumn and winter. In order to determine phytoplankton ecosystem responses to various physical and biological processes on a seasonal scale, we used Empirical Orthogonal/Eigen Function (EOF) analysis to investigate the covarying spatiotemporal patterns of: marine-sourced biomarkers and terrestrial-sourced biomarkers in surface suspended particles, a biomass indicator (Chl *a*), water-mass indicators [sea surface temperature (SST), sea surface salinity (SSS), nutrients], and a hydrodynamic indicator [total suspended solids at surface/bottom water, (TSS_S and TSS_B)]. The results identified six physical-biological coupling modes that influence seasonal variations in marine phytoplankton ecosystems within the energetic strait system. Additionally, an in-depth understanding of the coupling between physical process and lipid biomarker signals from suspended particles in the contemporary marine environment can offer valuable insights for interpreting ancient sediment records of phytoplankton ecosystem evolution in the TS.

Key words: lipid biomarkers, phytoplankton biomass, community structure, physical processes, the western Taiwan Strait

Citation: Liu Zitong, Tao Shuqin, Ye Xiang, Wang Aijun, Ran Chang, Wu Shuilan, Jiang Zhen, Wu Junwen. 2024. Spatiotemporal variations of phytoplankton in the Taiwan Strait using lipid biomarkers and the potential influencing factors. Acta Oceanologica Sinica, 43(11): 68–87, doi: 10.1007/s13131-024-2380-1

1 Introduction

Since pre-industrial times, global warming has become increasingly evident as atmospheric CO_2 concentrations have risen from 2.8×10^{-4} μL/L to 4×10^{-4} μL/L (NOAA, 2021; Showstack, 2013). The marine biological pump is an important pathway for removing and fixing atmospheric CO_2 (Turner, 2015). The efficiency of the marine biological pump is highly dependent on marine phytoplankton, the main primary producers in the ocean. The production and community structure of marine phytoplankton changes the ability of the biological pump to regulate the carbon cycle (Archer et al., 2000; Ding et al., 2010). Meanwhile, marine primary production, or phytoplankton biomass, is influenced by multiple physical-chemical factors, such as upwelling, river plumes, and eddies (Barlow et al., 2017; Chen et al., 2021; Falkowski et al., 1991; Gong et al., 2003; Liu et al., 2019; Ryan et al., 2010). The nutrient structure of the stratified water column is controlled by upwelling, thereby regulating the growth of phytoplankton in the vertical direction (Gong et al., 2003). The

Foundation item: The National Key Research and Development Program of China under contract No. 2019YFE0124700; the Scientific Research Foundation of Third Institute of Oceanography, MNR under contract Nos 2019018 and 2019017; the National Natural Science Foundation of China under contract Nos 42076038, U22A20585 and 41776099; the Guangdong Basic and Applied Basic Research Foundation under contract No. 2021A1515011886; the STU Scientific Research Start-Up Foundation for Talents under contract No. NTF18011.

*Corresponding author, E-mail: taoshuqin@tio.org.cn; wujw@stu.edu.cn

three-dimensional salinity and temperature structures can indicate the overlapping areas of river plumes and upwelling regimes, which in turn influence the distribution of size-fractionated chlorophyll *a* (Chl *a*) (Liu et al., 2019). Meanwhile, abundant nutrients in the water column are brought by eddy pumping, leading to a substantial enhancement in production (Barlow et al., 2017). These factors can enhance the coupling between the mixed layer and the bottom boundary layer to some extent, altering the nutrient structure and subsequently impacting the growth environment of phytoplankton, resulting in differences in production and community structure. The marginal seas, as hotspots in terms of organic carbon (OC) sequestration and biological pumps, represent only 8% of the area of the global ocean, but account for more than 20% of the open ocean CO_2 uptake and ~90% of the marine OC burial (Burdige, 2005; Field et al., 1998; Zhao et al., 2021). Therefore, studying the factors influencing phytoplankton biomass in marginal seas can help in understanding the response of the biological pump on different spatiotemporal scales and predicting the coastal environment under future climate change scenarios.

In general, various indicators have been used to track changes in phytoplankton biomass or community structure, including Chl *a* (Tang et al., 2004; Yamaguchi et al., 2013), photosynthetic pigments (Mineeva, 2021; Zhong et al., 2020), and lipid biomarkers (Bi et al., 2018; Ding et al., 2019; Wu et al., 2016). Compared to Chl *a* and other photosynthetic pigments, lipid biomarkers are superior in terms of chemical stability, which is more suitable for studying the long timescales of phytoplankton community structure changes (Ding et al., 2010). Indeed, lipid biomarker compounds such as sterols and long-chain alkenones have been widely used to elucidate organic matter sources and environmental fate in aquatic systems (Bianchi and Canuel, 2011; Brassell et al., 1986; Wu et al., 2016). They maintain a relatively intact carbon structure under the processes of degradation and diagenesis (Ding et al., 2010), which allows us to effectively decipher the biomass and community of phytoplankton in aquatic ecosystems (Hernandez et al., 2008; Hernandez-Sanchez et al., 2010). They also can identify the source and determine the fate of organic matter in the ocean; for example, sterols have been applied to reconstruct the abundance of diatoms and dinoflagellates in the Routheast Pacific (Tolosa et al., 2008), the East China Sea (ECS) (Jeng and Huh, 2004; Sicre et al., 1994), the Yellow Sea (Kannan et al., 2012), and the South China Sea (SCS) (Li et al., 2012, 2014). Alkenones have been applied to reconstruct haptophytes in the eastern Bering Sea (Harada et al., 2003), the ECS (Nakanishi et al., 2012), the SCS (Li et al., 2012, 2014), and the Japan Sea (Lee et al., 2014). Brassicasterol (24-methylcholesta-5, 22E-dien-3β-ol), dinosterol (4α, 23, 24-trimethyl-5α-cholest-22-en-3β-ol), and C_{37} alkenones are particularly useful lipid biomarkers in aquatic systems, representing the biomass of diatoms, dinoflagellates, and haptophytes, respectively, in the ocean's euphotic layer (Schubert et al., 1998; Xing et al., 2011; Zhao et al., 2006).

The Taiwan Strait (TS) is a strong-current, high-energy system linking the ECS and the SCS, and is influenced by various physical factors including the strong ocean currents, coastal upwelling, and distal and proximal river plumes (Tao et al., 2022). Meanwhile, a "narrow conduit effect" makes the strait highly energetic and serves as a crucial pathway for the exchange of water masses and materials between the adjacent marginal seas (Chen et al., 2006; Jiao et al., 2018; Wu et al., 2015). The physical processes in such a transitional setting play a great role in regulating the local biogeochemistry, including nutrient availability, carbon cycling and marine production (e.g., phytoplankton, zooplankton and fish) (Lan et al., 2014; Liu et al., 2019; Tao et al., 2022; Zhong et al., 2020). Previous studies based on Chl *a* and other photosynthetic pigments in waters of the TS suggested that seasonal changes of phytoplankton biomass are controlled by several physical and biological factors (e.g., water mass characteristics, light transmittance, community structure, and nutrient levels, etc.) in relation to the ecological niches of the different algae and their different responses to the physical processes (Hong et al., 2011a; Tseng et al., 2020; Zhong et al., 2020). Previous studies have also focused on lipid biomarkers to interpret phytoplankton distributions in sediments of the TS, indicating that the composition of these biomarkers are influenced by primary production from the upper water column and regional hydro- and sedimentary dynamics in the TS (Tao et al., 2022). However, sediment results reflect long-term climate averages (several years to decades), rather than shorter-term variations like seasonal or inter-annual scales, due to the high spatiotemporal variability of marine physical processes in the TS (Gan et al., 2009; Hong et al., 2009; Hu et al., 2010; Huang et al., 2015; Jan et al., 2002) . This study aims to enhance the accuracy of biomarker methods in reconstructing phytoplankton biomass and community structures by incorporating short timescale biological signals, which helps explain phytoplankton dynamics from a new perspective and confirming previous research results. In this study, spatiotemporal patterns of phytoplankton biomass and community structures are revealed using phytoplankton-sourced biomarkers extracted from suspended particle material across the four seasons from 2019 to 2020 in surface waters of the TS, in order to investigate how marine physical processes impact regional phytoplankton dynamics at a resolution of seasonal timescales.

The objectives of this study are: (1) to investigate the spatiotemporal distributions of biomarkers in suspended particles from TS surface seawater to reconstruct phytoplankton biomass and community structures, (2) to interpret the coupling between marine physical and biogeochemical processes using a novel Empirical Orthogonal/Eigen Function analysis (EOF) processing method and elucidate the intrinsic drivers responsible for spatiotemporal changes in biomarkers, and (3) to better understand changes in the evolution of phytoplankton biomass and community structure during the transition between northeast and southwest monsoons in the TS.

2 Materials and methods

2.1 *Study area*

The TS has wide shelves dominated by distal Changjiang River and Zhujiang River fluvial sources (Fig. 1a). Substantial loads of terrestrial material from several medium to small sized rivers such as the Minjiang, Jiulong and Hanjiang rivers discharge into the western TS. On the eastern side, a large number of small mountainous rivers in Taiwan produce disproportionately high sediment yields (Liu et al., 2013). A "narrow conduit effect" is produced by the terrain barriers on both sides, and is significantly amplified by the orientation of the currents in the same direction as the monsoon winds (Zhong et al., 2020). The TS is mainly influenced by two major monsoon systems. During the monsoon transition period, the northeasterly and southwesterly winds alternate, impacting the physical system of the TS (Yang et al., 2021). During October–April, the TS is affected by the strong northeast (NE) monsoon, which mainly forms three ocean currents: the southward Min-Zhe Coastal Current (MZCC) along the western TS, and the northward South China Sea Warm Current

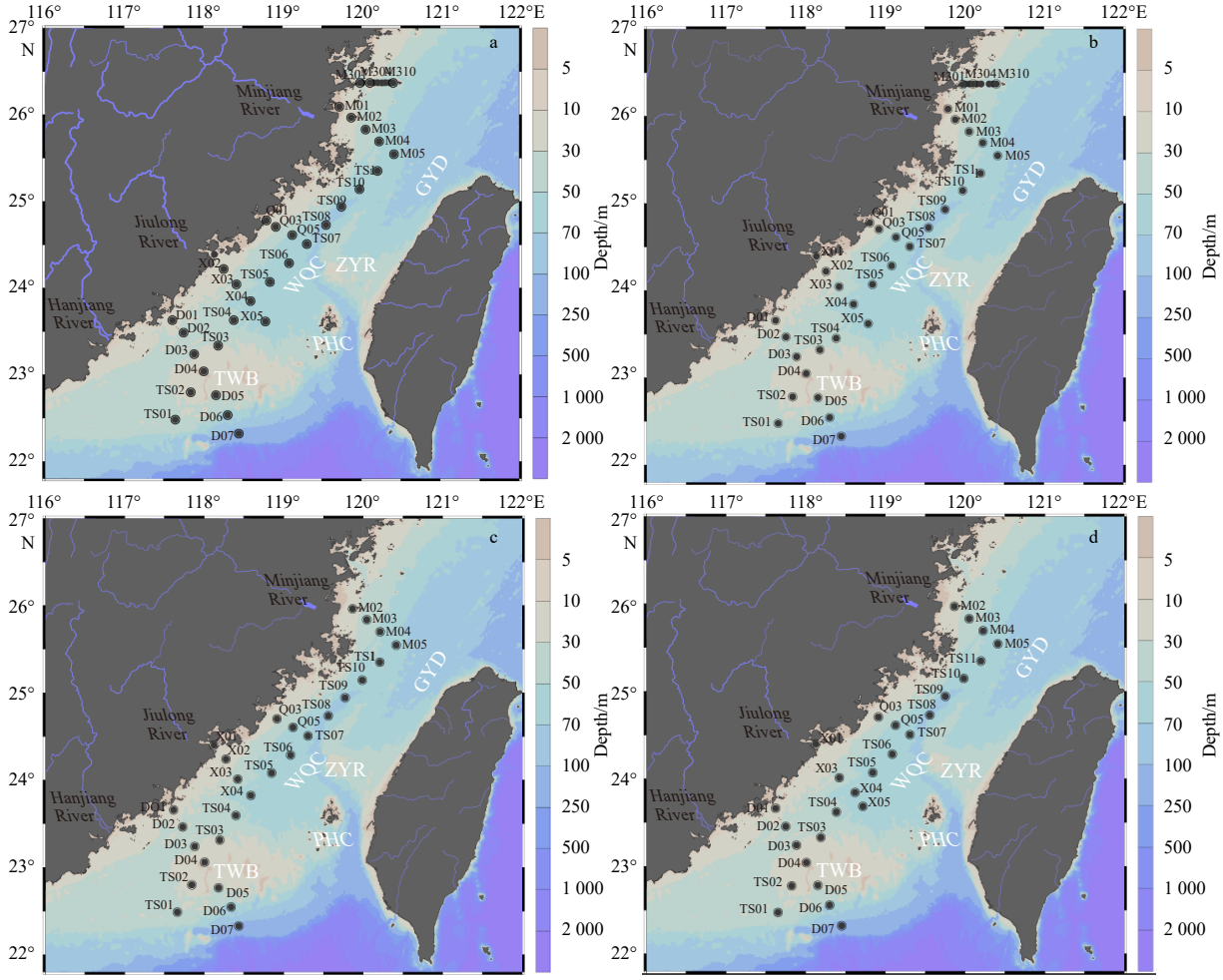

Fig. 1. Maps of sampling sites (black dots) from 4 cruises in the TS during 2019–2020: spring (a), summer (b), autumn (c), and winter (d). Rivers are depicted as turquoise lines. TWB: Taiwan Banks, PHC: Penghu Channel, ZYR: Zhanyun Rise, GYD: Guanyin Depression, WQC: Wuqiu Channel.

(SCSWC) and Kuroshio intrusion water (KW) along the middle and eastern TS. The low-temperature and low-salinity MZCC moves from north to south, affecting most of the waters on the west side of the TS, and reaches as far south as near Dongshan Island. The east of the strait is significantly affected by the SCSWC from south to north. During winter, the current of the TS presents a confrontation between the east and the west. The southwest (SW) monsoon (June–August) drives the SCSWC and KW northward into the TS (Zhong et al., 2020). The central and northern part of the TS is mainly controlled by warm currents from the south, and the net water flux in the whole strait northeastward. The combination of wind-driven currents and complex bottom topography create the upwelling regions, such as the Dongshan upwelling, Pingtan upwelling, Taiwan Bank upwelling, and Penghu upwelling (Hong et al., 2009; Hu et al., 2001; Liu et al., 2019; Tang et al., 2002). The coastal upwelling usually occurs along the west coast, triggered by the prevailing SW monsoon winds which supply a large amount of nutrients resulting in high levels of marine production in the TS (Tseng et al., 2020; Zhong et al., 2020).

2.2 *Field sampling*

Field surveys (measurements and sampling) were conducted onboard the R/V *Haijian 203* during spring (May 2020), summer (August 2020), autumn (October 2019) and winter (December 2019) cruises. The sampling locations are shown in Fig. 1. Suspended particle samples for lipid biomarker analyses were obtained by filtration on Whatman GF/C filters (150 mm diameter). After filtration, samples were stored at –20℃.

2.3 *Hydrological and chemical parameter analyses*

Seawater samples were collected and vertical profiles of hydrological parameters such as sea surface temperature (SST) and sea surface salinity (SSS) were measured *in situ* with a conductivity–temperature–depth (CTD) system (Seabird SEB 19).Their standard deviations are shown in Table 1.

Nutrients: 100 mL seawater samples were filtered through a pre-washed cellulose acetate membrane (0.45 μm) and measured following the method of Grasshoff et al. (1999). Nutrients (nitrate, phosphate and silicate) were measured with a QUAATRO nutrient analyzer at the Third Institute of Oceanography (TIO), Ministry of Natural Resources of China. The detection limits were 0.02 μmol/L (nitrate), 0.01 μmol/L (phosphate) and 0.02 μmol/L (silicate). Additional 500 mL seawater samples, from both the surface and bottom, were filtered through a 0.45 μm filter, oven-dried at 40℃, and weighed to calculate the concentration of total suspended solids (TSS). Finally, ~2 L seawater samples from the surface were filtered through pre-combusted Whatman GF/F filters, freeze-dried and weighed for measuring bulk particulate organic matter (POM) characteristics, including

Table 1. Overview of mean and standard deviation of various parameters of four seasons required for this research

Parameter	Spring	Summer	Autumn	Winter
SST/℃	22.0 ± 2.0	27.4 ± 1.4	24.1 ± 1.6	19.1 ± 1.6
SSS	32.2 ± 2.3	34.0 ± 0.3	32.5 ± 1.7	32.2 ± 1.6
TSS_S/(mg·L^{-1})	18.8 ± 4.4	14.8 ± 8.1	6.3 ± 5.3	9.8 ± 6.5
TSS_B/(mg·L^{-1})	21.8 ± 6.5	23.6 ± 13.1	11.8 ± 10.0	16.9 ± 12.6
C/N ratio	7.0 ± 3.1	7.4 ± 2.3	8.6 ± 2.6	6.7 ± 1.7
$\delta^{13}C$/‰	−23.6 ± 1.6	−24.6 ± 1.4	−24.9 ± 1.3	−25.1 ± 1.2
N/P ratio	48.9 ± 42.2	30.4 ± 21.6	20.6 ± 10.0	23.8 ± 14.5
Silicate concentration/(μmol·L^{-1})	1.7 ± 2.1	4.0 ± 4.1	11.2 ± 11.9	1.7 ± 2.1
n-$C_{26+28+30}$ FAs/(ng·L^{-1})	10.5 ± 10.6	11.0 ± 14.7	7.3 ± 4.4	8.2 ± 5.2
n-$C_{28+30+32}$ alkanols/(ng·L^{-1})	27.9 ± 26.0	25.8 ± 31.0	6.0 ± 9.4	13.4 ± 12.8
n-$C_{29+31+31}$ alkanes/(ng·L^{-1})	19.4 ± 17.3	25.9 ± 36.2	15.3 ± 12.4	30.2 ± 40.0.3
Brassicasterol/(ng·L^{-1})	1 157.7 ± 1 459.2	115.6 ± 51.0	59.2 ± 68.0	89.8 ± 54.1
Dinosterol/(ng·L^{-1})	137.8 ± 234.5	49.5 ± 51.0	9.1 ± 12.0	11.9 ± 4.6
C_{37} alkenones/(ng·L^{-1})	49.1 ± 63.4	95.6 ± 197.4	3.4 ± 7.3	6.5 ± 6.4
Cholesterol/(ng·L^{-1})	425.2 ± 312.1	322.4 ± 196.6	108.6 ± 112.2	131.8 ± 80.6
ΣPB/(ng·L^{-1})	1 295.5 ± 1 650.7	165.1 ± 93.0	68.3± 79.2	101.7± 55.9
Chl *a* concentration/(mg·m^{-3})	3.4 ± 3.9	1.3 ± 0.9	1.3 ± 0.5	1.8 ± 1.0

Note: The C/N ratio and N/P ratio used in this study is nitrate molar concentration ratio.

particulate organic carbon (POC) content, particulate nitrogen (PN) content, and $\delta^{13}C$ analyses. These parameters were conducted using an elemental analyzer in the Stable Isotope Platform/Community Lab at TIO. The precision of OC content measurements was better than ±0.2%.

Chl *a* concentrations were measured by a multi-parameter water quality *in-situ* analyzer produced by YSI Company (model YSI EXO2). The instrument was calibrated before the voyages to ensure reliable data. Note that, the field Chl *a* data only includes spring, summer and autumn, while Chl *a* data in the winter is sourced from satellite-born radiometer using the monthly average value at a spatial scale of a 4 km × 4 km grid.

2.4 *Biological parameters analyses*

The target lipid biomarkers include marine sourced sterols, plant wax derived *n*-alkanes, *n*-alkanols and *n*-fatty acid methyl esters (*n*-FAMEs). Suspended particle samples for lipid biomarker analysis were collected in spring (40 sites), summer (40 sites), autumn (28 sites), and winter (28 sites) (Fig. 1). The methods for extraction, purification and isolation of target biomarkers have been modified from Tao et al. (2022). In brief, filtered samples were spiked with an appropriate amount of a non-internal standard mixture and then subjected to ultrasonic extraction with a mixture of dichloromethane (DCM) and methanol (MeOH). Afterward, a "neutral" fraction and an "acidic" fraction were extracted from the hydrolyzed solution separately after adjusting the pH of solution. The "neutral" fraction was further separated by SiO_2 column chromatography into two fractions: the nonpolar fraction eluted by 8 mL hexane containing *n*-alkanes and the polar fraction eluted by 12 mL DCM/MeOH (95:5, *v*/*v*) containing plant wax *n*-alkanols and marine phytoplankton sterols (Brassicaterol, Dinosterol and C_{37} alkenones). Before measurement, the various components in both fractions underwent several steps including concentration, derivatization, transesterification, and elution purification. *n*-alkyl lipid and sterol identifications were determined with a Thermo gas chromatography-mass spectrometer (GC-MS) by comparing retention times with the standards. Quantification was performed with an Agilent 7890B GC instrument using an HP-1 column and He as carrier gas. The average relative standard deviation (%) was less than 10%.

2.5 *Empirical Orthogonal/Eigen Function analysis (EOF)*

In order to investigate the mechanisms controlling seasonal changes in phytoplankton biomass and community structures in the TS, a multivariate EOF analysis was used to assess their correlation (standardized covariance) with different environmental parameters using Matlab_R2021b software. This technique is based on internal correlations (Resio and Hayden, 1975), which presents the statistical characteristics of a group of data through the spatial or temporal correlation of the data (Du and Liu, 2017; Liu et al., 2019; Tao et al., 2022; Yang et al., 2021). The eigenmodes were sorted based on the quotient between each mode's eigenvalue and the sum of all eigenvalues. Mode 1, which has the largest eigenvalue, explains the majority of the covariance (correlation) in the dataset as a percentage shown in Table 2. Subsequent modes, such as Modes 2 and 3, explain less correlation

Table 2. Summary of EOF results of seasonal primary physical regimes

Season	Mode 1	Mode 2	Mode 3
Spring (68.8%)	43.2%	13.9%	11.7%
	MZCC (promoting algal bloom events)	SCSWC, gathering in the south	water colum mixing
Summer (58.7%)	32.9%	14.8%	11.0%
	coastal upwelling	Kuroshio invasion from northeastern part	river plume (proximal & distal)
Autumn (65.8%)	28.6%	19.2%	18.0%
	bottom resuspension, high turbidity inhibits the PP	MZCC in the northern part of the study area during monsoon transition	residual upwelling
Winter (72.7%)	39.7%	18.7%	14.3%
	strong MZCC, the farthest southward journey can reach Dongshan Island	water colum mixing	bottom resuspension

Note: The percentage in the parenthesis is the cumulative percentage of the first 3 modes. The description below each mode percentage is the dominant physical regime.

compared to Mode 1, and soon (Liu et al., 2019). The eigenvector of each variable can be divided into positive and negative groups based on their sign. Specifically, the variable with the largest absolute value of the eigenvector is generally recognized as the dominant factor influencing the correlation of the pattern. The eigenweightings of a particular eigenmode show the spatial or temporal patterns of that mode.

3 Results

3.1 *Hydrological (SST, SSS) and chemical (nutrients) parameters in TS surface water during the four seasons*

In spring, SST ranged from 18.9℃ to 26.5℃ [average = (22.0 ± 2.0)℃, n = 40] and SSS ranged from 26.8 to 34.6 (average = 32.2 ± 2.3, n = 40). Cold, fresh water with lower SST and SSS was observed in the coastal areas on the west side of the strait, with a trend of increasing SST and SSS towards the south (Figs S1a and S2a). In summer, SST ranged from 23.9℃ to 29.9℃ [average = (27.4 ± 1.4)℃, n = 40] and SSS ranged from 33.1 to 34.5 (average = 34.0 ± 0.3, n = 40). Higher SST and SSS were observed in the southern TS, suggesting the intrusion of the SCSWC. However, the SST along the western coastline remained relatively low, indicating the influence of upwelling in these areas (Fig. S1b). In autumn, the SST and SSS ranged from 21.2℃ to 26.7℃ [average = (24.1 ± 1.6)℃, n = 28], 28.5 to 34.2 (average = 32.5 ± 1.7, n = 28), respectively. The distributions of SST and SSS were similar to spring, with lower SST and SSS values observed in the estuaries and higher values in the south (Figs S1a, S1c, S2a and c). Note that, the convergence of high and low temperature waters in autumn appears in a more southern location compared to spring, suggesting a stronger northeast monsoon in autumn compared to spring (Figs S1a and c). In winter, the SST ranged from 16.3℃ to 23.0℃ [average = (19.1 ± 1.6)℃, n = 28] and the SSS ranged from 27.7 to 34.5 (average = 32.2 ± 1.6, n = 28). On the west side of the TS, low SST and SSS appears in the coastal area due to a dominant influence of the MZCC (Figs S1d and S2d). However, relatively high SST and SSS were also observed in the southern TS, indicating that the SCSWC still has a dominant impact on the hydrological distribution of the southwestern strait during winter (Figs S1d and S2d).

The concentration of nitrate (NO_3^-) in surface seawater of the TS ranged from 0.3 μmol/L to 8.6 μmol/L [average = (1.4 ± 1.3) μmol/L, n = 40] in spring, 0.2 μmol/L to 9.2 μmol/L [average = (1.3 ± 1.4) μmol/L, n = 40] in summer, 0.3 μmol/L to 27.9 μmol/L [average = (7.6 ± 7.8) μmol/L, n = 28] in autumn, and 1.9 μmol/L to 35.7 μmol/L [average = (13.0 ± 8.2) μmol/L, n = 28] in winter, respectively. The average concentration of nitrate showed a minor variation from spring to summer. However, there was a significant increase in the average concentration during autumn and winter, exceeding the levels observed in spring and summer. This indicates a decrease in the utilization of nutrients by phytoplankton, leading to a surplus of nitrate during autumn and winter. The spatial distribution of nitrate in spring was similar to that in summer. Higher values were observed exclusively in the Minjiang River Estuary area (Figs S3a and b). In autumn, nitrate in the TS was replenished. High nitrate concentrations were observed in the estuaries and the central region of the study area, extending beyond the mouth of the Minjiang River (Fig. S3c). These areas of high concentrations also extend further outward during the winter (Figs S3c and d). The relatively high concentration of nitrate in estuaries throughout the four seasons highlights the importance of riverine inputs to nutrient supplies and emphasizes that its impact should not be ignored.

The concentration of phosphate (PO_4^-) in surface seawater of the TS ranged from 0.01 μmol/L to 0.25 μmol/L [average = (0.08 ± 0.07) μmol/L, n = 30] in spring, 0.01 μmol/L to 0.12 μmol/L [average = (0.05 ± 0.03) μmol/L, n = 40] in summer, 0.03 μmol/L to 1.31 μmol/L [average = (0.37 ± 0.36) μmol/L, n = 28] in autumn, and 0.04 μmol/L to 1.49 μmol/L [average = (0.64 ± 0.38) μmol/L, n = 28] in winter. Compared to nitrate, the average concentration of phosphate was significantly lower during the observation period. However, its seasonal variability was similar to that of nitrate, with lower concentrations in spring and summer and a gradual increase in autumn and winter. Spatially, there were no high-concentration areas observed in either spring or summer when phosphate was depleted (Figs S3e and f). Similar to nitrate, phosphate was also replenished during autumn and winter. High concentrations were observed in estuaries (especially Quanzhou Bay) and offshore areas (Figs S3g and h). Indeed, river inputs and coastal flows from the MZCC can deliver abundant phosphates, resulting in excess phosphate along the west side of the study area.

The concentration of silicate (SiO_3^{2-}) in surface seawater of the TS ranged from 0.02 μmol/L to 10.8 μmol/L [average = (1.7 ± 2.1) μmol/L, n = 40] in spring, 0.2 μmol/L to 21.3 μmol/L [average = (4.0 ± 4.1) μmol/L, n = 36] in summer, 0.2 μmol/L to 44.3 μmol/L [average = (11.2 ± 11.9) μmol/L, n = 28] in autumn, and 0.6 μmol/L to 48.2 μmol/L [average = (17.3 ± 12.1) μmol/L, n = 28] in winter. Seasonal changes suggested that the utilization rate of silicate by phytoplankton was highest in spring and lowest in winter. The distribution of silicate in spring is similar to summer; high concentrations only occurred in the estuaries, particularly in the Minjiang River and Jiulong River estuaries (Figs S3i and j). In autumn and winter, silicates were replenished, similar to the other nutrients, and concentrated in various estuarine areas. However, differing from nitrate and phosphate distributions, silicates have a weaker increase towards the open sea and primarily impact the estuarine areas (Figs S3k and l). The correlations between nutrients can be seen in Fig. S4.

The N/P ratios used in this study are calculated as Nitrate/Phosphate molar concentration. N/P ratios ranged from 6.2 to 156.0 (average = 48.9 ± 42.2, n = 33) in spring, from 4.6 to 96.3 (average = 30.4 ± 21.6, n = 40) in summer, from 6.5 to 49.5 (average = 20.6 ± 10.0, n = 28) in autumn, and from 8.0 to 76.1 (average = 23.8 ± 14.5, n = 28) in winter. The N/P ratios are applied to the statistical analysis of *T-S* plots and EOF.

The variations in environmental parameters in the TS during the four seasons indicate the seasonal impacts of various physical and biogeochemical processes. The *T-S* map effectively identifies distinct clusters of water characteristics based on temperature, salinity, and nutrients, which is consistent with previous findings (Zhong et al., 2020). These clusters correspond to seasonal ocean currents, river plumes, upwelling, and other phenomena (Fig. 2). In spring, water mass characteristics such as high SST, high SSS, and few nutrients, indicate the influence of the SCSWC, while low SST, low SSS, and abundant nutrients suggest the influence of ZMCC. Additionally, relatively high SST and low SSS in a water mass can be attributed to the river plume. Thus, the TS are influenced by three water masses: the SCSWC, MZCC, and the river plume (Figs 2a and b). Water masses that exhibit less distinct characteristics or have signatures that are a mix of identified water masses are classified as mixed water. By analogy, it can be inferred that the water mass characteristics in autumn and winter are primarily influenced by the two major water masses, the SCSWC and ZMCC (Figs 2e–h). However, the upwelling of low SST, high SSS, nutrient-rich water is a unique feature in summer and is likely to dominate water mass charac-

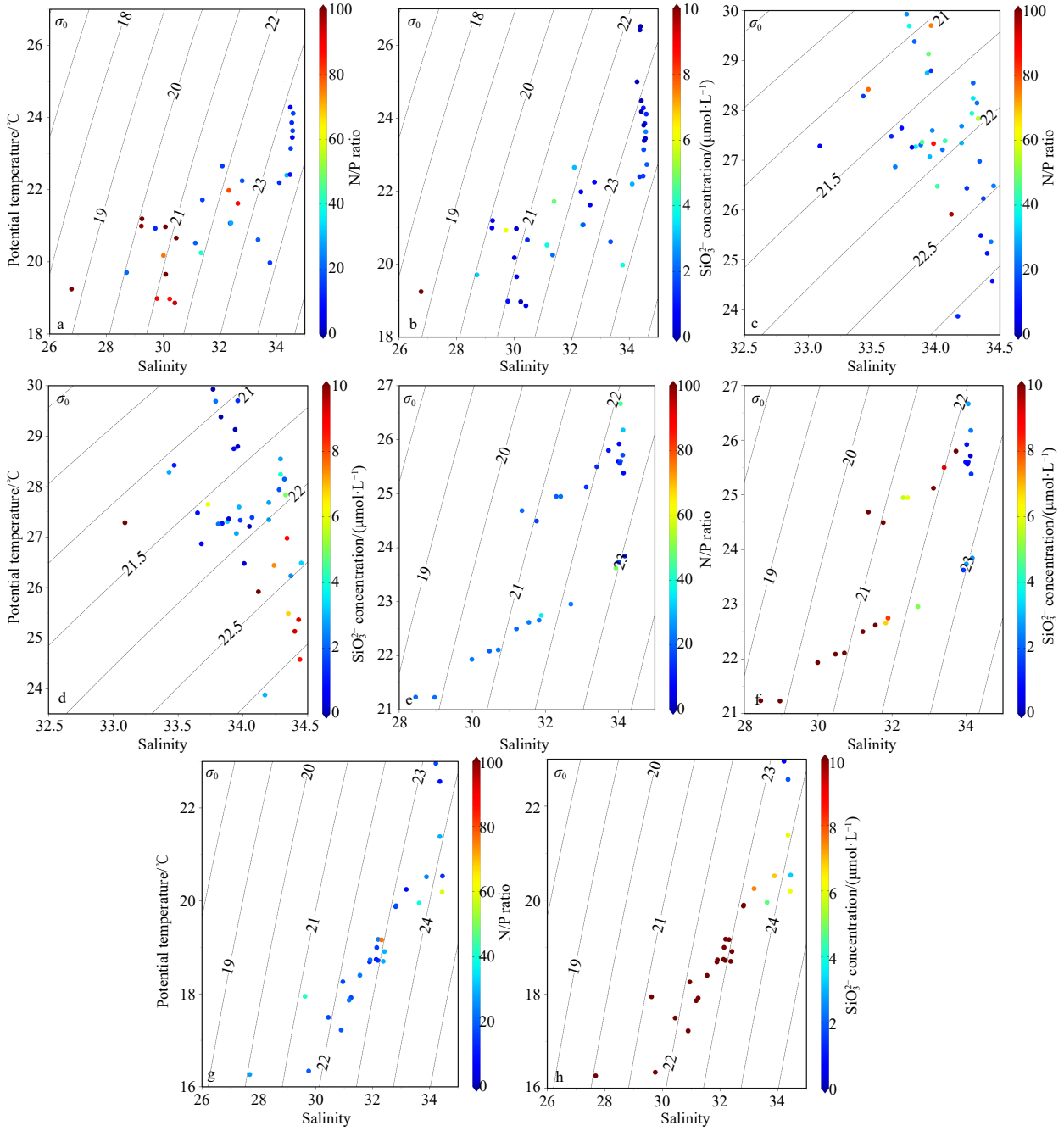

Fig. 2. Temperature-salinity-N/P (T-S-N/P) and temperature-salinity-silicate (T-S-Si) diagram of surface water during spring (a, b), summer (c, d), autumn (e, f), winter (g, h) in the TS. N/P ratio stands for Nitrate/Phosphate molar concentration ratio.

teristics during this season (Figs 2c and d).

3.2 *Lipid biomarker distributions*

3.2.1 *Terrestrial biomarkers*

Odd long-chain (n-$C_{29+31+33}$) alkanes, even long-chain (n-$C_{28+30+32}$) alkanols, and long-chain (n-$C_{26+28+30}$) FAs are mainly sourced from terrestrial higher plant wax lipids, and have been widely used to trace the source of terrestrial OM and determine its fate in marine settings (Tao et al., 2022).

The concentration of odd long-chain (n-$C_{29+31+33}$) alkanes in TS surface waters ranged from 4.6 ng/L to 82.6 ng/L in spring, 3.5 ng/L to 202.4 ng/L in summer, 5.1 ng/L to 46.4 ng/L in autumn, and 6.3 ng/L to 210.9 ng/L in winter. The highest average concentration was observed in winter, while the lowest was observed in autumn. Throughout the observation period, higher odd long-chain alkane concentrations were consistently observed in the estuaries, which is attributed to the abundance of terrigenous OM brought in by river inputs. Additionally, a slight increase in concentration was noted in the southern part of the strait during spring and autumn (Figs 3a–d).

The concentration of even long-chain (n-$C_{28+30+32}$) alkanols in TS surface waters ranged from 4.0 ng/L to 110.8 ng/L in spring, 4.2 ng/L to 142.3 ng/L in summer, 0.5 ng/L to 51.7 ng/L in autumn, and 3.1 ng/L to 66.3 ng/L in winter. The highest average concentration was observed in spring, while the lowest was observed in autumn. Similar to n-$C_{29+31+33}$ alkanes, the n-$C_{28+30+32}$ alkanols did not exhibit a clear seasonal pattern during our

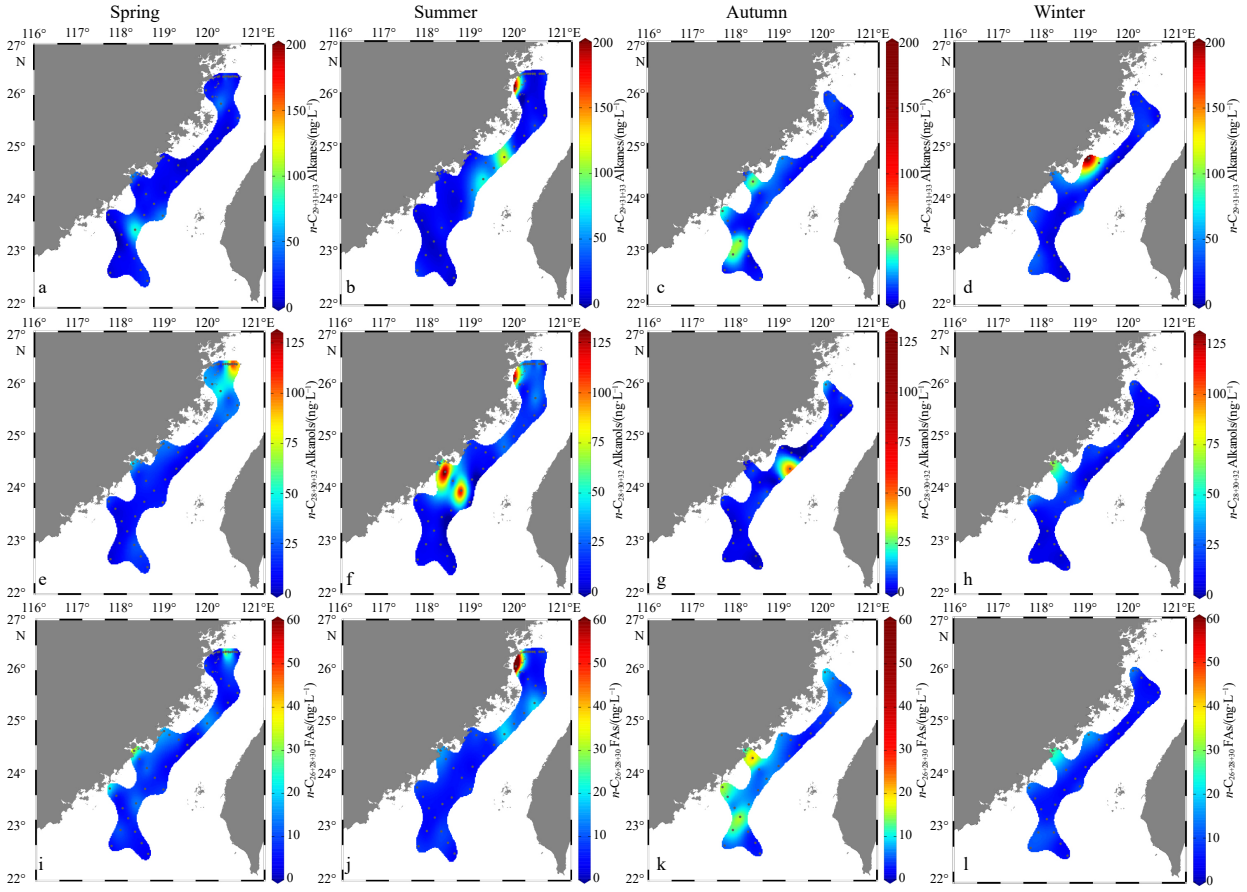

Fig. 3. Distribution of terrestrial biomarkers (ng/L) in surface suspended particles in the TS during 2019–2020 (a–l): $C_{29+31+33}$ alkanes (Figs 3a–d); $C_{28+30+32}$ alkanols (Figs 3e–h); $C_{26+28+30}$ FAs (Figs 3i–l).

observation period. The highest value occurred in the offshore area of the Minjiang River Estuary on the west side of the TS, with a secondary high value near the Jiulong River Estuary (Figs 3e–h).

The concentration of long-chain (n-$C_{26+28+30}$) FAs in TS surface waters ranged from 1.9 ng/L to 58.3 ng/L in spring 3.5 ng/L to 98.3 ng/L in summer, 2.5 ng/L to 20.7 ng/L in autumn, and 3.5 ng/L to 27.5 ng/L in winter. The average concentration of n-$C_{26+28+30}$ FAs remained consistently low across all four seasons, with minimal variations between seasons. High concentrations were consistently observed in several estuarine areas on the west side throughout most seasons. The second-highest levels were found in the central and northern parts of the strait during spring and summer (Figs 3i–l).

3.2.2 *Marine biomarkers*

The spatial distributions of four marine biomarkers (brassicasterol, dinosterol, C_{37} alkenones and cholesterol) showed very large seasonal variability. In particular, concentrations of marine lipid biomarkers in spring were significantly higher than those in other seasons (Fig. 4).

The concentration of brassicasterol in TS surface seawater ranged from 54.4 ng/L to 5 446.8 ng/L [average = (1 157.7 ± 1 459.2) ng/L, n = 40] in spring, 49.1 ng/L to 218.6 ng/L [average = (115.6 ± 51.0) ng/L, n = 40] in summer, 6.9 ng/L to 283.7 ng/L [average = (59.2 ± 68.0) ng/L, n = 28] in autumn, and 41.9 ng/L to 332.5 ng/L [average = (89.8 ± 54.1) ng/L, n = 28] in winter. The elevated brassicasterol concentrations were primarily due to the occurrence of red tide events, leading to exceptionally high levels of marine-sourced biomarkers overall. The highest values during both spring and summer were located in the region stretching from the mouth of the Minjiang River seaward to offshore (Figs 4a and b). Additionally, during the summer, there was a secondary high concentration area at the offshore site south of Nanri Island (Fig. 4b). During autumn and winter, the high concentration area of brassicasterol shifted towards the southern region and offshore sites (Figs 4c and d).

The concentration of dinosterol in TS surface seawater ranged from 8.6 ng/L to 926.6 ng/L [average = (137.8 ± 234.5) ng/L, n = 40] in spring, 10.5 ng/L to 199.0 ng/L [average = (49.5 ± 51.0) ng/L, n = 40] in summer, 1.3 ng/L to 63.3 ng/L [average = (9.1 ± 12.0) ng/L, n = 28] in autumn, and 4.1 ng/L to 23.9 ng/L [average = (11.9 ± 4.6) ng/L, n = 28] in winter. The variations in dinosterol concentrations were in agreement with those of brassicasterol: the maximum and minimum values appear in spring and autumn, respectively. During the spring and summer, the highest values were generally observed in the Minjiang River Estuary (Figs 4e and f). The distribution of dinosterol was similar to that of brassisterol in autumn and winter, showing a propensity of higher concentrations toward the outer sea (Figs 4g and h). Meanwhile, the concentrations of dinosterol were very low in this period.

The concentrations of C_{37} alkenones in TS surface seawater ranged from 1.0 ng/L to 274.0 ng/L [average = (49.1 ± 63.4) ng/L, n = 40] in spring, 0.8 ng/L to 900.3 ng/L [average = (95.6 ± 197.4) ng/L, n = 40] in summer, 0.2 ng/L to 38.2 ng/L [average = (3.4 ± 7.3) ng/L, n = 28] in autumn, and 1.2 ng/L to 26.3 ng/L [average = (6.5 ± 6.4) ng/L, n = 28] in winter. Seasonally, C_{37} alkenone concentrations were variable, showing a rapid increase from spring to summer and then a sharp decrease in autumn, suggesting a positive correla-

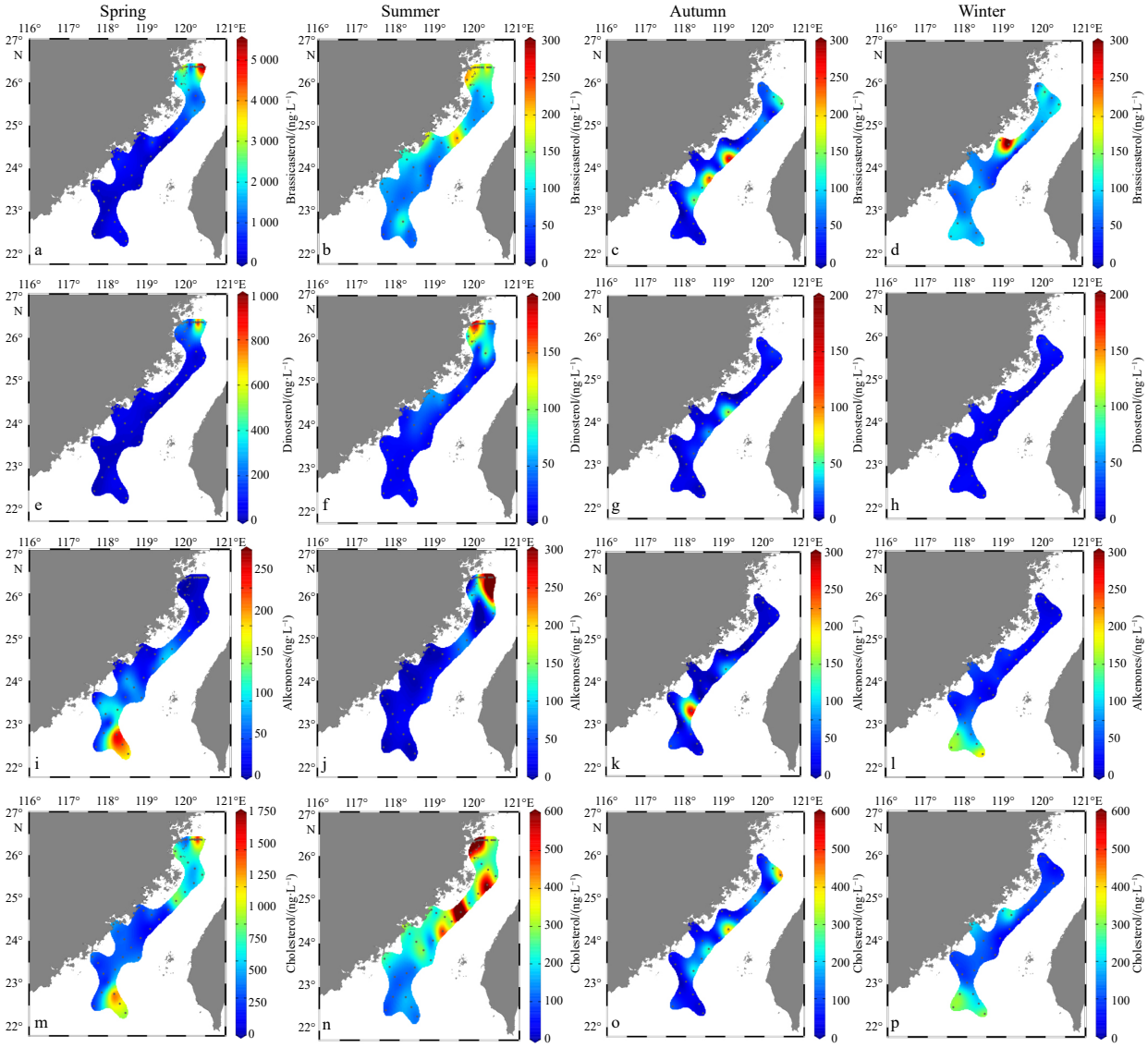

Fig. 4. Distribution of marine biomarkers (ng/L) in surface suspended particles in the TS during 2019–2020 (a–p): brassicasterol (Figs 4a–d); dinosterol (Figs 4e–h); C_{37} alkenones (Figs 4i–l); cholesterol (Figs 4m–p). Note that the biomarker concentration color-bar scale in spring is differentiated from other seasons due to the red tide events of planktonic algae during the spring cruise.

tion between C_{37} alkenone concentration and temperature. The distribution of C_{37} alkenones showed significant spatiotemporal differences; higher concentrations in spring were primarily concentrated in the southern region (Fig. 4i), while the higher concentrations in summer were shifted towards the north (Minjiang River Estuary) (Fig. 4j). Correspondingly, the lowest concentrations appeared in autumn and winter compared to spring and summer (Figs 4k and l).

The concentrations of cholesterol in TS surface seawater ranged from 58.4 ng/L to 1 515.1 ng/L [average = (425.2 ± 312.1) ng/L, n = 40] in spring, 92.6 ng/L to 853.9 ng/L [average = (322.4 ± 196.6) ng/L, n = 40] in summer, 18.5 ng/L to 435.3 ng/L [average = (108.6 ± 112.2) ng/L, n=28] in autumn, and 42.6 ng/L to 310.8 ng/L [average = (131.8 ± 80.6) ng/L, n = 28] in winter. The distribution of cholesterol was consistent with that of brassicasterol and dinosterol, further indicating that biomass was limited in autumn. In spring, higher cholesterol concentrations were observed in both the northern and southern regions of the channel (Fig. 4m). However, the highest values of cholesterol were mainly observed in the northern TS during summer (Fig. 4n). Similar to brassicasterol and dinosterol, higher concentrations of cholesterol tend to be shifted towards the offshore area and the southern TS during autumn and winter; specifically, higher concentrations were observed in the offshore sites during autumn and in the southern regions during winter (Figs 4o and p).

3.3 *Eigen function analysis of the physical-chemical-biological dataset during four seasons*

In order to determine the impact of diverse physical processes on the phytoplankton community of the TS in different seasons, EOF analysis was used to examine the correlation among the 15 independent variables during each season, including 2 bulk OM parameters (C/N molar concentration ratio and $\delta^{13}C$), 3 groups of terrestrially-sourced biomarker (the concentrations of n-$C_{27+29+31}$ alkanes, n-$C_{28+30+32}$ alkanols, and n-$C_{26+28+30}$ FAs), 4 marine-sourced biomarkers (phytoplankton-derived brassicasterol, C_{37} alkenones, dinosterol, and zooplankton-derived cholesterol), and 6 marine environmental parameters (SST,

SSS, silicates, N/P ratio, Chl *a* and TSS). In addition, TSS in bottom layers was included in the EOF analysis for autumn and winter as an indicator of strong resuspension observed as higher turbidity or TSS concentrations at the seafloor and the sediment-water interface. The results indicate a strong correlation among the 15 variables, with the first three eigen modes accounting for over 58% of the data co-variability. Comparison of the seasonal EOF structures reveals the highest correlation in winter (72.7%) and the lowest in summer (58.7%) (Table 2). Since the objectives of this study are related to phytoplankton biomass and community structure, our description of the results will focus on the co-variability of phytoplankton-sourced lipid biomarkers in relation to other variables.

In spring, Mode 1 explains 43.2% of the co-variability among different physical, chemical and biological parameters (Table 2). Based on the sign of the eigenvectors, all variables have been divided into two groups. The negative group includes C_{37} alkenones, SST and SSS, and the remaining variables are in the positive group (Fig. 5a). The spatial patterns of this grouping are shown in the contour plot of the eigenweightings, in which the positive areas follow the northwestern coast corresponding to the location of the colder and less salty MZCC water (Figs 6a and S1a). Notably, terrestrially-sourced *n*-alkanols and *n*-$C_{26+28+30}$ FAs, marine phytoplankton-sourced brassicasterol and dinosterol, zooplankton-sourced cholesterol, Chl *a*, N/P ratios and the surface turbidity index (TSS_S) are prominent eigenvectors in the positive group (Fig. 5a). Therefore, this mode emphasizes that the MZCC regime (lower temperature, lower salinity) dominates hydrographic, chemical and biological properties of the TS in spring, especially in the northwestern TS. As an extension of the distal Changjiang River input, MZCC intrusion can bring inorganic N-enriched and high-turbidity water to the TS, along with increased primary production (high Chl *a* concentration) regardless of the specific terrestrial and marine sources. Mode 2 explains 13.9% of the co-variability (Table 2), and is dominated by the water mass indicators SST and SSS in the positive group and

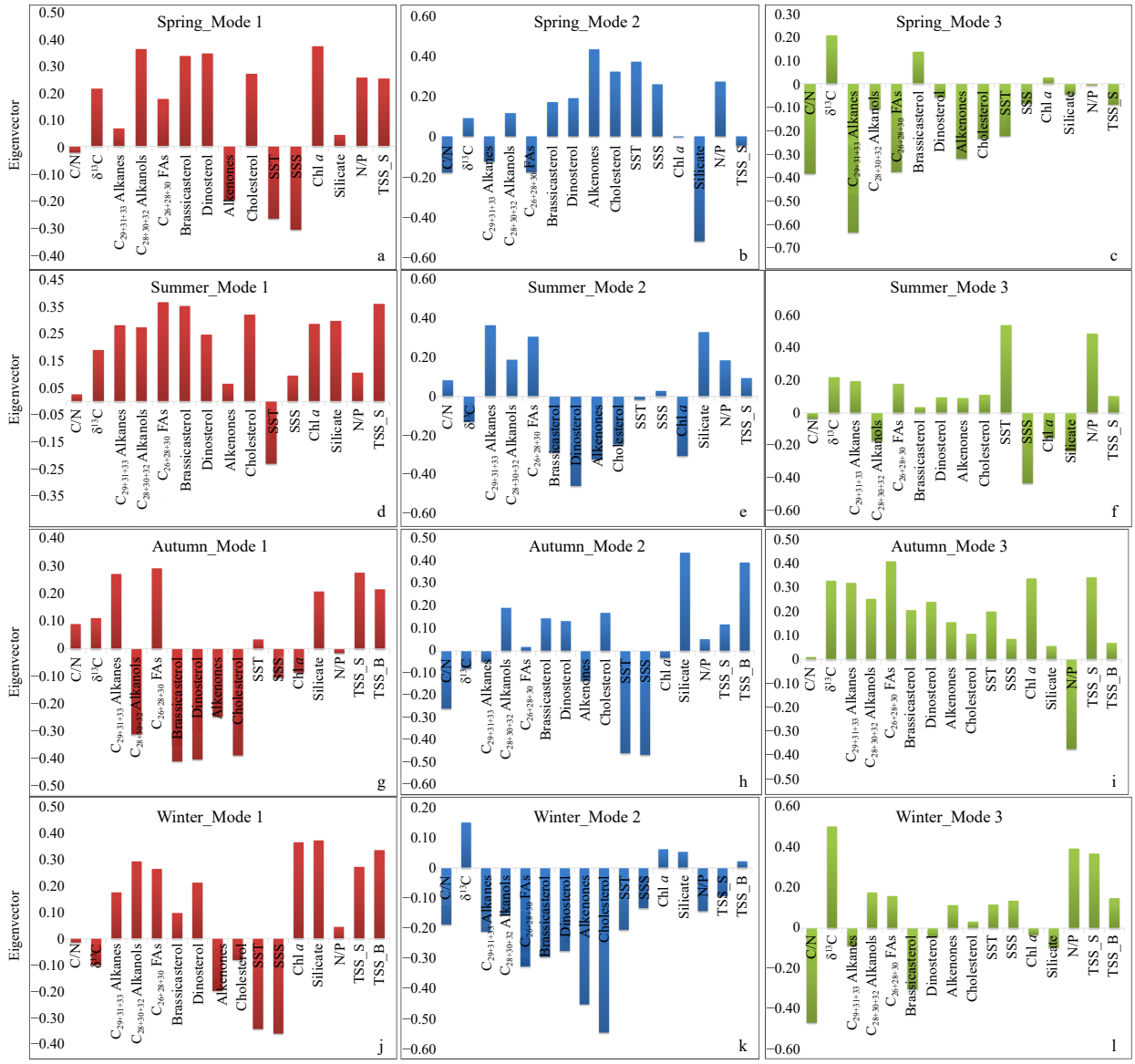

Fig. 5. Contour plot of eigenvectors of Modes 1, 2, 3 in four seasons (a–l). Each frame shows the groupings of the 15 variables (16 variables in winter) as indicated by the sign of the eigenvectors. The line is the zero contour that separates positive and negative contoured areas.

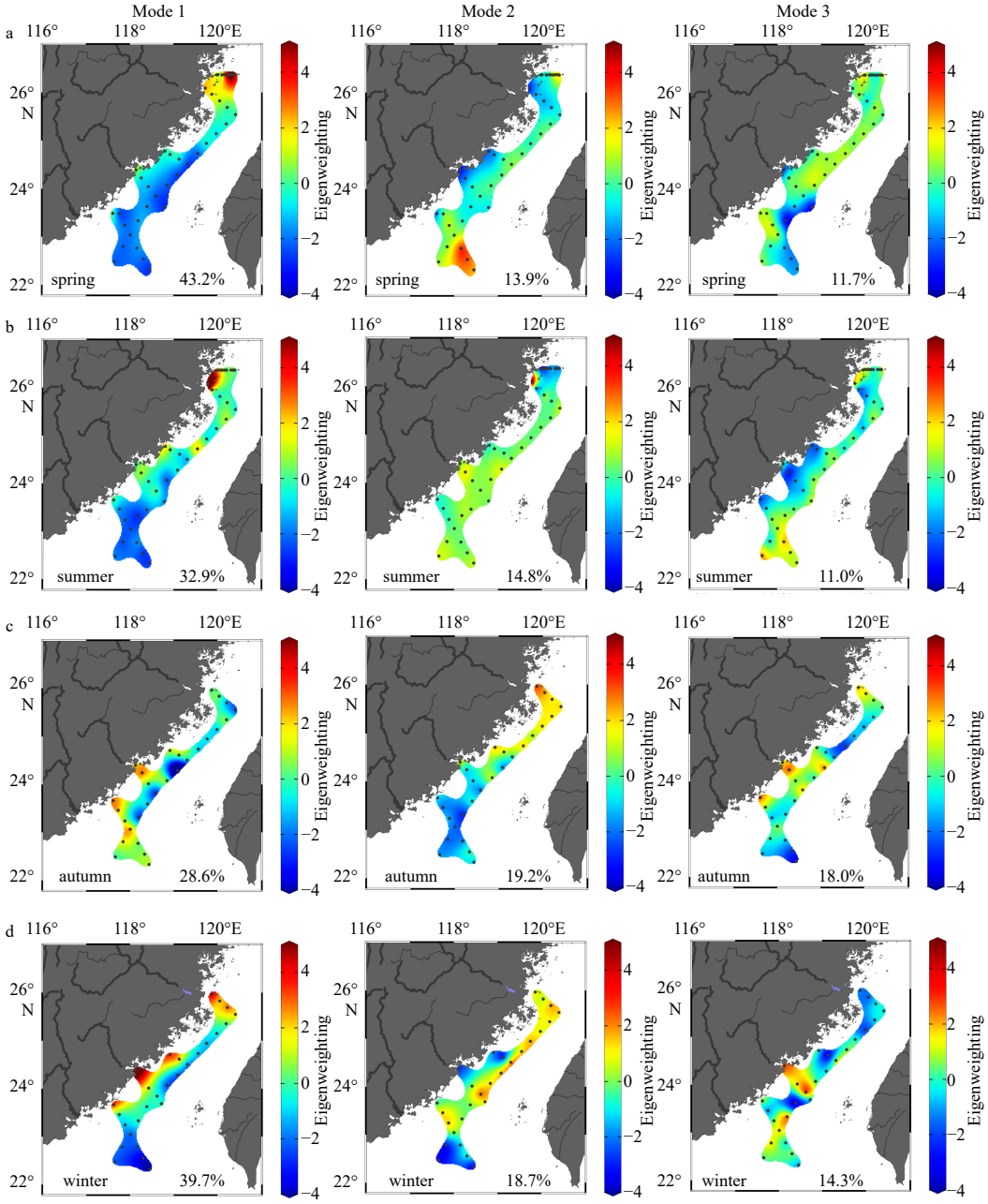

Fig. 6. Contour plot of eigenweightings of Modes 1, 2, 3 in spring (a), summer (b), autumn (c) and winter (d). The percentage values reflect the correlation explained by each mode. The contours of eigenweightings show the spatial pattern of the corresponding grouping.

the land-sourced nutrient silicate in the negative group (Fig. 5b). The positive regions in the contoured eigenweightings of this mode follow the southwestern and center region of the TS (Fig. 6a) corresponding to the location of the warmer and saltier SCSWC water (Figs S1a and S2a) with low levels of land-derived nutrients (Figs S3a, e and i). Thus, this mode highlights the oligotrophic SCSWC regime as a secondary physical process affecting the physical and biochemical properties of the study area in spring, with a stronger influence in the southeastern and central regions of the TS. Furthermore, zooplankton-derived cholesterol and haptophyte-derived C_{37} alkenones are prominent factors in the positive group compared to other marine-sourced biomarker variables (Fig. 5b), suggesting that SCSWC intrusion is a dominant physical process that is tightly coupled with biological feedback from zooplankton and haptophytes in the southern TS.

Mode 3 explains 11.7% of the co-variability (Table 2); there are only two prominent variables ($\delta^{13}C$ and brassicasterol) in the positive group, while the rest of the variables fall into the negative group (Fig. 5c). The negative regions in the contoured eigenweightings of this mode follow the areas of the Taiwan Banks (TWB) and estuaries, corresponding to the locations of stronger hydrodynamic conditions (Figs 1a and 6a). Thus, this mode suggests the mixing of saline shelf water with warmer and less salty river plumes as a tertiary physical process affecting physical and biochemical properties in spring, with a significant influence near the river mouth and TWB. Moreover, terrestrially-sourced biomarkers such as *n*-$C_{29+31+33}$ alkanes and *n*-$C_{26+28+30}$ FAs are the dominant biomarker variables in this mode, indicating a coupling of water mixing process with the presence of terrestrial OM.

In summer, the first mode explains 32.9% of the co-variability

among various physical, chemical and biological parameters (Table 2). This mode shows an association of Chl *a*, marine-sourced biomarkers and SSS in the positive group, and an inverse relationship with SST (Fig. 5d). This implies a colder and saltier upwelling influence on higher primary biomass contributions. The spatial pattern of this grouping (Fig. 6b) highlights the positive areas along the western coastal region in the TS. Within the positive regions of the mode, there are four high-eigenweighting areas located offshore southwest to Nari Island and outside the Minjiang River and Jiulong River estuaries, which align with the locations of coastal upwelling as noted in previous studies (Hong et al., 2009; Hu et al., 2001; Liu et al., 2019). Moreover, diatom-sourced brassicasterol is prominent in the upwelling mode compared to other marine-sourced biomarkers, indicating that diatoms are the primary contributors to the phytoplankton community in the upwelling regimes of the western TS in summer. Additionally, silicate, terrestrially-sourced biomarkers, and TSS_S also exhibit high absolute values of eigenvectors, underscoring the influence of eutrophic river plumes characterized by significant amounts of terrestrial material in these upwelling regimes near the coast. Mode 2 explains 14.8% of the co-variability (Table 2). This mode shows an association of all the marine-sourced biomarkers and Chl *a* in the negative group, while terrestrially-sourced biomarkers and the land-derived nutrient silicate are prominent in the positive group (Fig. 5e). The negative regions in the coutoured eigenweightings of this mode follow the northeastern region in the TS (Fig. 6b). Thus, this mode more than likely suggests the intrusion of the bottom branch of the Kuroshio Current into the ECS shelf during the summer, corresponding to more marine-sourced biomarkers. The increased biomass is likely caused by this branch which can extend to the 50 m isobath near the coast during summer, impacting offshore ecological processes (Yang et al., 2017) and suggesting that the Kuroshio invasion from the northeastern region is a dominant physical process tightly coupled with biological feedback from marine phytoplankton in this mode (Table 2). Mode 3 explains 11.0% of the co-variability in the dataset. SST and N/P are dominant in the positive group, while silicate and SSS exhibit larger absolute values in the negative group (Fig. 5f). The spatial pattern of this grouping highlights the positive areas offshore of the Minjiang River Estuary and the southeast part of the TWB (Fig. 6b). These areas correspond to the dispersal zones of the Minjiang River and Zhujiang River plumes in summer, indicating both proximal and remote river plumes as sources of less saline water entering the TS. The latter is driven by the distal Zhujiang River plume mixing with SCSWC as it crosses the TWB and enters the TS in summer (Lee et al., 2023; Liu et al., 2019; Yang et al., 2021). Additionally, all lipid biomarker signals are less pronounced in this mode, showing the identified river plumes have little impact on the biomass of phytoplankton.

In autumn, Mode 1 explains 28.6% of the co-variability. This mode shows an association of two terrestrially-sourced biomarkers, silicate and TSS, which are dominantly in the positive group whereas the marine-sourced biomarkers are in the negative group (Fig. 5g). The positive regions in the contoured eigenweightings follow the river mouths and the southern part of the study area (Fig. 6c). In this mode the addition of the bottom turbidity indicator (TSS_B) suggests that the resuspension of bottom sediments leads to increased turbidity, coinciding with a low abundance of marine-soured biomarkers. This suggests that the resuspension of bottom materials is a primary physical process affecting both physical and biochemical properties in autumn, which limits phytoplankton growth in the study area (Table 2). Mode 2 explains 19.2% of the co-variability. The eigenstructure (groupings and eigenweighting patterns) is similar to that of Mode 1 in spring (Figs 6a and c, 5a and h), indicative of the influence of the MZCC following the same interpretation. In contrast to the MZCC mode observed in spring, silicate and TSS_B exhibit the highest absolute value of eigenvectors in the positive group, while Chl *a* and both terrestrially- and marine-sourced biomarkers are not significant in this mode (refer to Fig. 5h). In autumn, the influence of the MZCC is limited to the northwestern TS (as shown in Fig. 6c), playing a crucial role in transporting land-sourced nutrients and sediment into the TS. However, the coupling of MZCC processes with biological signals such as Chl *a* and biomarker concentrations appears to weaken. Despite potential similarities in physical processes between spring and autumn, seasonal differences are evident. Mode 3 explains 18.0% of the co-variability. There is only one prominent variable (N/P ratio) in the negative group, while the rest of the variables fall into the positive group (Fig. 5f). This implies a low N/P water mass influence on higher biomass contributions. The spatial pattern shows the positive areas are located offshore of the TWB and Dongshan Island and outside the Jiulong River Estuary (Figs 1 and 6c), which align with the locations of coastal upwelling regimes as noted in previous studies (Hong et al., 2009; Hu et al., 2001; Liu et al., 2019). In contrast to upwelling regimes characterized by low temperatures and high salinities in summer, the colder and less salty MZCC results in upwelling areas in autumn exhibiting relatively high temperatures and salinities. The influence of this physical process in autumn is clearly evident in the southern part of the TS. Thus, this mode suggests the residual upwelling as a tertiary physical process affecting biochemical properties in autumn, with strong biological (biomarkers and Chl *a*) signals.

In winter, Mode 1 explains 39.7% of the co-variability in the dataset (Table 2). The eigenstructure is similar to that of Mode 1 during spring and Mode 2 during autumn (Figs 6a, c and d, 5a, h and j), indicative of the influence of the MZCC following the same interpretation. It is worth mentioning that TSS concentrations showed positive behavior (Fig. 5j), indicating an increase in turbidity. The positive regions in the contoured eigenweightings indicate its prevelance coastal areas, extending as far south as Dongshan Island (Fig. 6d). Mode 2 explains 18.7% of the co-variability. The eigenstructure is similar to the Mode 3 of spring (Figs 6a, 6d, 5c and 5k), indicative of the influence of mixing water masses following the same interpretation. Unlike the Mode 3 of spring, the negative regions in the contoured eigenweightings of this mode follow the southern and estuarine (Jiulong River and Quanzhou Bay) regions corresponding to the location of stronger hydrodynamic and biological conditions (Figs 6d and 5k), and this coupling mode is obviously more beneficial to the biological process. Mode 3 explains 14.3% of the co-variability (Table 2), and is dominated by $\delta^{13}C$, N/P and TSS in the positive group while C/N and brassicasterol are in the negative group (Fig. 5l). The positive regions follow the Jiulong River Estuary to offshore (Fig. 6d). It is worth noting that this spatial pattern is similar to the resuspension mode in autumn (Fig. 5g). However, the inhibition of biological processes by turbidity may be relatively less intense in this mode, as the responses of the three species of phytoplankton to environmental variables are quite different. The restriction on the growth of diatoms may be the greatest.

These findings highlight the significant impact of a monsoon climate on physical forcings and processes in the TS. In winter, strong NE monsoon winds have propelled the MZCC, leading to enhanced water column mixing and the generation of larger waves that triggered high turbidity from bottom resuspension. The transition from spring to autumn saw a shift in the influence

of monsoon winds. In spring, the water becomes warmer with the influence of the SCSWC becoming more pronounced, and nutrients are recovered from the MZCC. Water column mixing remains a crucial factor. In summer, coastal upwelling induced by the strong SW monsoon winds is a dominant physical process. River plumes also dominated biogeochemical features in the summer due to summer floods and typhoons. Autumn witnessed increased wave energy as the NE monsoon winds intensified, leading to further resuspension. The NE monsoon also intensifies the impact of the MZCC during autumn. In this transitional season, upwelling may have persisted in the TS as well.

4 Discussion

4.1 *Biomass and community structure of phytoplankton in the TS revealed by lipid biomarkers*

4.1.1 *Spatiotemporal variations of phytoplankton-sourced lipid biomarkers*

During the observation period of our cruise, we encountered a red tide event in spring. As a result, the concentration of marine biomarkers was exceptionally high. The mean concentrations of brassicasterol and dinosterol in spring were 10 times and 2.8 times higher, respectively, than in other seasons (Table 1). Wu et al. (2016) found that the average concentration of brassicasterol in suspended particulate matter of the ECS during summer was 6 times higher than in spring, and the concentration of dinosterol was 3 times higher. This is different from our results, and suggests that the impacts of episodic events (e.g., red tides) can cause a high level of phytoplanktonderived biomarker concentrations. Brassicasterol and dinosterol showed a similar spatial trend, with high-concentration areas in the northwest of the study area in spring and summer, and also in the central region of the study area in autumn and winter. However, the spatial distribution of C_{37} alkenones exhibited a contrasting pattern between spring and summer. In spring, the highest value was observed in the southern region, while the northern region had the highest value in summer. The concentrations of C_{37} alkenones during summer can reach levels comparable to the concentration of the most abundant brassicasterol. Variability in the C_{37} alkenone concentration of suspended particulates has been observed seasonally and spatially in the ECS, SYS and Japan Sea, illustrating that higher haptophyte biomass, as indicated by higher C_{37} alkenone concentrations in surface seawater, likely occurs in summer and autumn in the East Asia coastal areas along the northwest Pacific marginal seas (Lee et al., 2014; Wu et al., 2016). The concentration of phytoplankton biomarkers was lower in autumn and winter compared to spring and summer. In particular, in areas with high turbidity such as the nearshore and estuarine regions, the concentration was notably low during these seasons (Figs 7c and d). This can lead to lower concentrations of marine-sourced biomarkers and Chl *a* during these two seasons, making their spatial distribution patterns tend to be higher at offshore sites.

Chl *a* has been widely used to estimate phytoplankton biomass (Yamaguchi et al., 2013). While the additional application of phytoplankton-derived lipid biomarkers as indicators of phytoplankton production has often exhibited a bias because lipids only account for <1% of bulk OM components, previous studies have shown that lipid biomarkers in surface suspended particles can provide insights into marine phytoplankton biomass (Dong et al., 2012; Hernandez et al., 2008; Wu et al., 2016). For example, three phytoplankton lipid biomarkers showed good correlations with Chl *a* in suspended particles of the West Pacific surface water (Dong et al., 2012), and a significant positive correlation between the sum of three biomarkers and Chl *a* was found in the ECS and the SYS (Wu et al., 2016), indicating they show a similar quantity of phytoplankton. To ensure the reliability of the reconstruction of phytoplankton biomass using lipid biomarkers in the TS, we performed a correlation analysis between the field Chl *a* values and phytoplankton-derived biomarker concentrations to assess the feasibility of using biomarkers as an indicator of phytoplankton biomass. The correlations showed a significant positive correlation of both brassicasterol & dinosterol *versus* Chl *a*, while C_{37} alkenones displayed little correlation. Thus, the sum of brassicasterol and dinosterol was defined as the sum of phytoplankton biomarkers (∑PB), and this metric showed a strong correlation with Chl *a* in our study area (Fig. 8). The correlation analysis between different phytoplankton biomarkers and Chl *a* showed that diatoms and dinoflagellates were the main contributors to phytoplankton biomass in the TS, supporting their importance to carbon sequestration in this area. Haptophytes were not the main contributors of phytoplankton biomass, and their impact on carbon sequestration from marine production is not significant. The relationships between biomarkers and Chl *a* suggest that phytoplankton-derived lipid biomarker indicators have good applicability in evaluating phytoplankton biomass and community in the TS.

4.1.2 *Phytoplankton biomass and community structure in the TS*

Diatoms (*Bacillariophyceae*) are prominent phytoplankton community members in eutrophic conditions and are responsible for most blooms worldwide (Sarthou et al., 2005), but they can also play a significant biogeochemical role in oligotrophic oceans (Scharek et al., 1999). Previous studies have suggested that the realized niche of diatom groups is the same during the SW and NE monsoon periods, both characterized by relatively low-temperatures, low-salinities and high-nutrient concentrations, and its niche breadth is broad (Zhong et al., 2020). This suggests diatoms can adapt well to various environmental changes and survive, thus typically having an advantageous position in the community. We observed that diatoms have a significant community advantage during all four seasons (Fig. 9). In addition, diatom-dominated phytoplankton communities are associated with high-nutrient, turbulent conditions such as vernal blooms in temperate latitudes (Bustillos-Guzmán et al., 1995; Latasa et al., 2010) and upwelling areas (Du and Peterson, 2018; Fawcett and Ward, 2011) as well as with high-nutrient, low-chlorophyll zones of the Southern Ocean (Gutiérrez-Rodríguez et al., 2020).

Based on the classification by Latasa et al. (2010), dinoflagellates belong to the eutrophic group; they often form blooms in estuaries and coastal areas around the world, and are generally considered as the “culprits” of harmful red tides. During our spring cruise, we encountered a red tide outbreak event which had high concentrations of dinosterol (a biomarker specific to dinoflagellates) (Figs 4e and 9a). Dinoflagellates exhibit a lack of response to the specific physical environment due to their high species diversity and wide range of ecological niches. The proportion of dinoflagellates was higher in warm seasons and closer to estuaries compared to offshore areas (Figs 9a and b).

Numerous studies have consistently shown that haptophytes exhibit a preference for environments characterized by high mean temperatures, high salinities, and oligotrophic conditions (Baumann et al., 2005; Kinkel et al., 2000; Wu et al., 2016; Zhong et al., 2020). In our study, we observed distinct seasonal variability in the distribution of haptophyte-sourced C_{37} alkenones (Figs 4i–l).

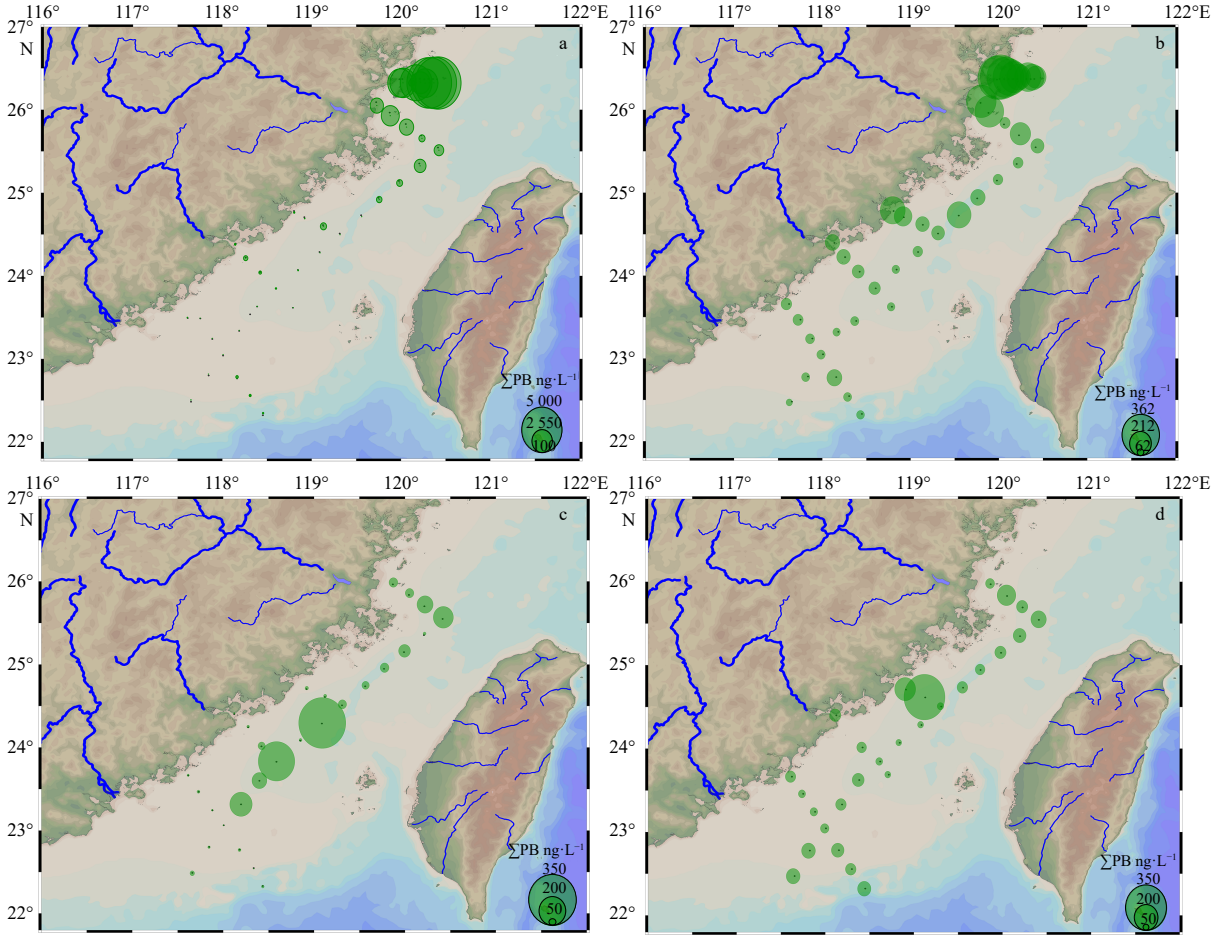

Fig. 7. Spacial variations of biomass revealed by the sum of brassicasterol, dinosterol of four seasons in the TS: spring (a), summer (b), autumn (c), winter (d). Bubble graph diameter is proportional to the ΣPB (ng/L). ΣPB was used to assess the biomass of phytoplankton expressed as the sum of dinosterol and brassicaterol contents.

Generally, more C_{37} alkenones indicated an enhanced presence of haptophytes in the southern part of the study area during spring, autumn, and winter (Figs 9a, c and d), and an absolute dominance of haptophytes in the northern part of the study area in summer (Fig. 9d). This is similar to the seasonal changes of the SCSWC and Kuroshio intrusions in the TS, and our findings are supported by the results of EOF analysis (Fig. 5e). The Kuroshio branch, which flows laterally from the northern side of the TS (Yang et al., 2017), may entrench Kuroshio-specific species of haptophytes in this area.

Compared to spring and summer, the growth of phytoplankton in autumn and winter may be restricted due to high turbidity caused by the muddy coastal current, low-runoff river plumes and bottom resuspension.

4.2 *Controlling factors on the spatiotemporal variability of phytoplankton production and community structure in the strait system*

A previous study has revealed that the distribution of phytoplankton in the TS is partially controlled by water masses, which are differentiated by temperature, salinity, and nutrient concentration (Zhong et al., 2020). Additionally, numerous studies have investigated the impact of distinct water masses on phytoplankton communities in various regions such as in the East Australian Current separation zone (Hassler et al., 2011), the western Arctic Ocean (Jin et al., 2017), and the ECS (Bi et al., 2018; Kang et al., 2016; Xu et al., 2019). Based on the EOF results, we identified the main physical process (the water regime) of the TS and its degree of influence during each season (Table 2). The complex interactions among physical forcing, water mass, nutrient dynamics, and phytoplankton ecology based on spatiotemporal patterns of lipid biomarkers have been controlled by various physical systems/processes. We further discuss the coupled relationship and seasonal differences between specific physical and biogeochemical processes.

4.2.1 *Six coupling modes between physical processes and biological signals based on EOF analysis*

Based on the results of the EOF analysis, the first three eigen modes collectively account for over 58% of the data co-variability, representing the important physical-biological coupling modes in each season. Comparison of the seasonal EOF structures shows the highest correlation in winter (72.7%) and the lowest in summer (58.7%) (Table 2), indicating that the zones in the TS impacted by physical processes exhibit greater complexity and variability in summer than in winter. However, the physical processes involved are diverse, and some can manifest in different seasons and maintain their impact on phytoplankton community structure. Therefore, we reorganized the results of EOF (regardless of season) and summarized six independent physical processes that have direct/indirect impacts on phytoplankton ecosystems (Table 2 and Fig. 5).

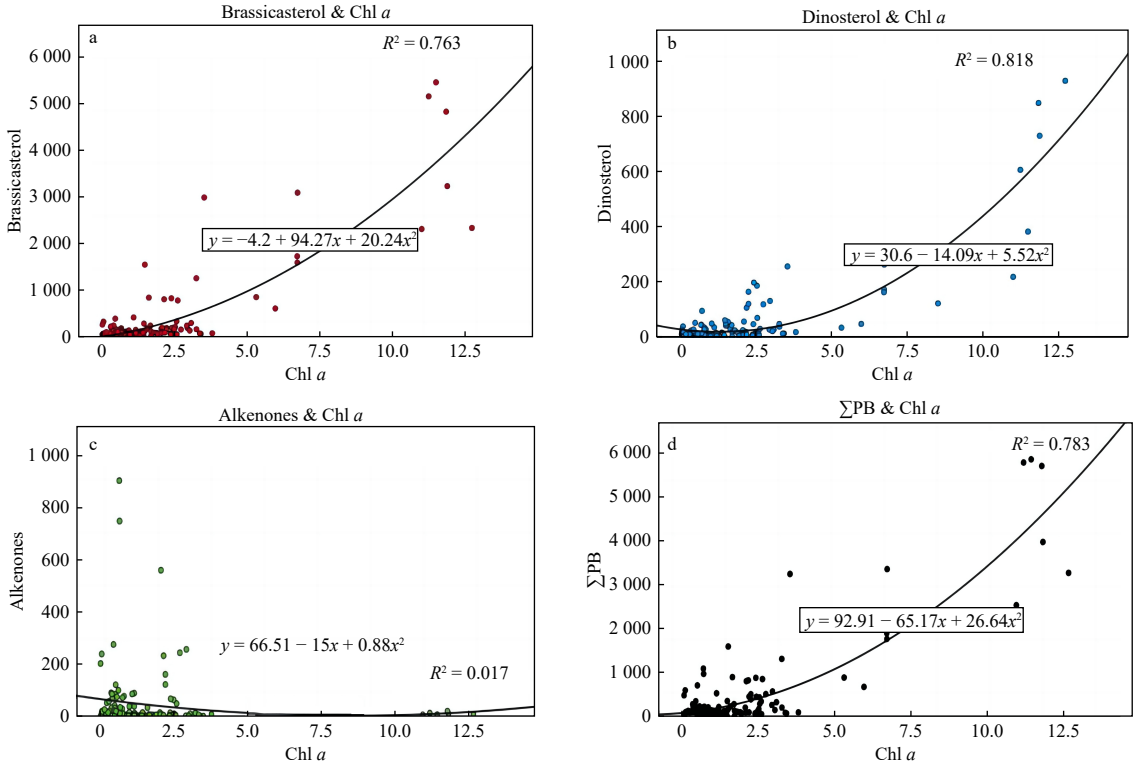

Fig. 8. Scatter plots of the correlation between three biomarkers (a, b, c) and the sum of brassicasterol and dinosterol (∑PB) (d) verse chlorophyll *a*. The curve represents the total fitting curve of the quadratic term.

The first physical-biological coupling mode is the MZCC impact mode, which is elucidated by Mode 1 in spring and winter, and Mode 2 in autumn. Although their impact areas may vary, they consistently influence phytoplankton communities. The eigenvector maps demonstrate that Chl *a*, diatom-derived brassicasterol and dinoflagellate-derived dinosterol are in the positive group, while haptophyte-derived C_{37} alkenones are in the negative group (Figs 5a, h and j). This suggests that the MZCC promotes the growth of phytoplankton, particularly diatoms and dinoflagellates, but inhibits the growth of haptophytes.

The second physical-biological coupling mode is the SCSWC impact mode, which can be explained by Mode 2 in spring. The eigenvector maps demonstrate that all three phytoplankton biomarkers co-vary in the positive group, but the response of haptophyte-derived C_{37} alkenones to this coupling mode is significantly greater than the other two (high eigenvector absolute value) (Fig. 5b). This suggests that the emergence of SCSWC has led to an increase in the biomass of haptophytes. The distribution of C_{37} alkenone concentrations in spring also reveals their peak occurrence in the southern region, which corresponds to the influence area of SCSWC (Figs 4i and 6a).

The third physical-biological coupling mode is the coastal upwelling impact mode, which can be explained by Mode 1 in summer and Mode 3 in autumn. Although they show some seasonal differences, their effects on phytoplankton communities are consistent. The eigenvector maps demonstrate that all biomarkers and Chl *a* are in the positive group with high absolute values (Figs 5d and i). These modes exhibit typical upwelling characteristics, which not only result in abundant land-sourced organic matter due to its proximity to the coasts but also significantly promote the biomass of marine phytoplankton by supplying nutrients through water column ventilation. It should be mentioned that in upwelling areas, diatoms exhibit a stronger response to upwelling compared to other phytoplankton groups.

The fourth physical-biological coupling mode is the river plumes impact mode, which can be explained by Mode 3 in summer. This coupling mode actually has no obvious promoting effect on phytoplankton groups, even though all marine-sourced biomarkers are in the positive group, while Chl *a* is in the negative group (Fig. 5f).

The fifth physical-biological coupling mode is the resuspension impact mode, which can be explained by Mode 1 in autumn and Mode 3 in winter. Although their impact areas may vary, they consistently influence phytoplankton communities. The eigenvector maps demonstrate that all marine-sourced biomarkers are in the negative group (Figs 5g and l). This suggests that the high turbidity effect caused by resuspension strongly limits the growth of phytoplankton. Thus, the resuspension mode is not conducive to more biomass.

The last physical-biological coupling mode is the Kuroshio invasion impact mode, which can be explained by Mode 2 in summer. The eigenvector maps demonstrate that all marine-sourced biomarkers and Chl *a* are in the negative group (this pattern explains the negative group) (Fig. 5e). This suggests that the Kuroshio invasion promotes the growth of all three phytoplankton groups.

4.2.2 *Seasonal controlling factors based on the correlations between phytoplankton biomarkers and the influence degree of specific physical process modes*

We have separated six distinct physical process patterns and gained some understanding of the response relationship between each pattern and biological signals. However, further understanding of the impact of each pattern on community composition is also essential. Hence, we conducted a correlation analysis between three phytoplankton-derived biomarkers, ΣPB, and

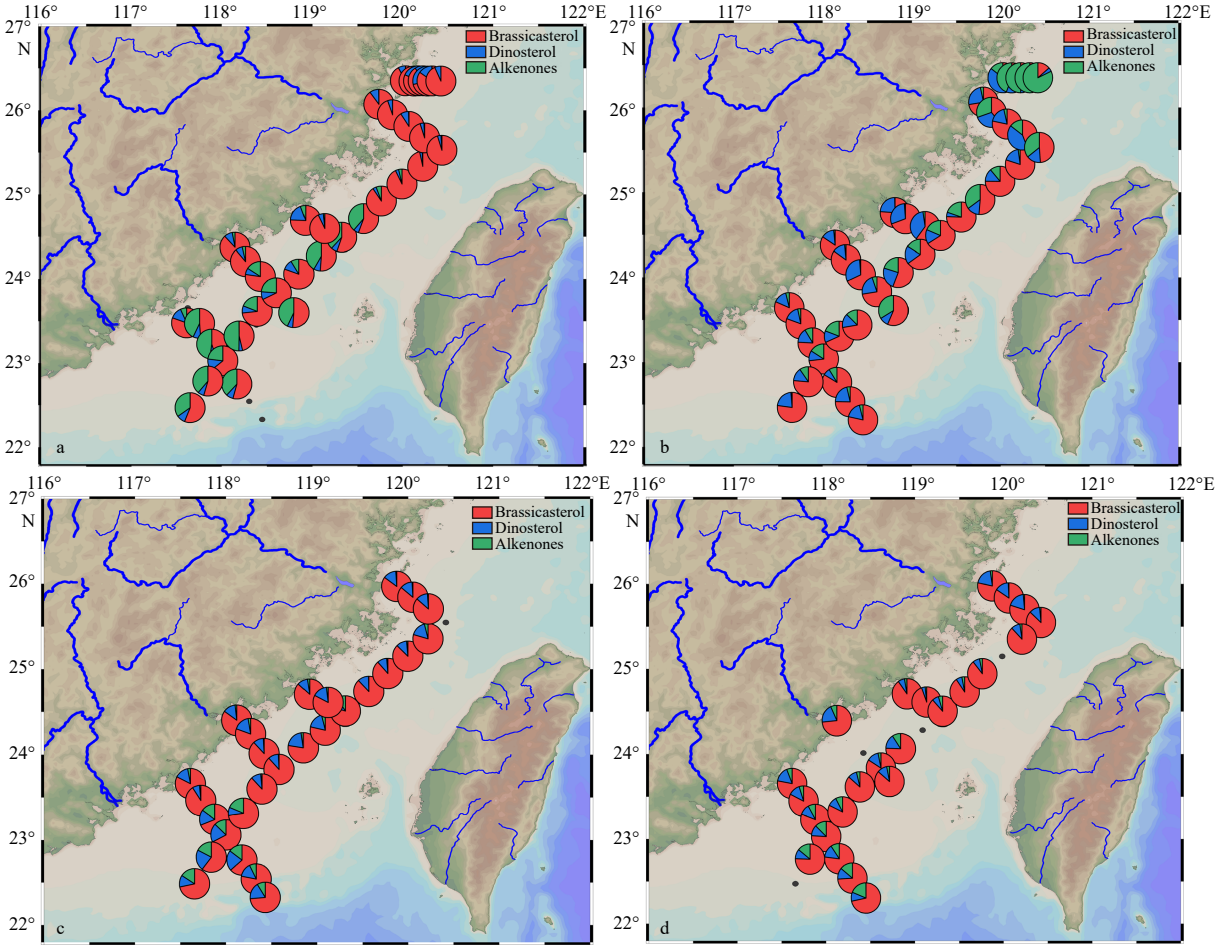

Fig. 9. Variations of surface phytoplankton compositions of four seasons in the TS: spring (a), summer (b), autumn (c), winter (d). Brassicasterol, dinosterol and C_{37} Alkenones represent diatoms, dinoflagellates, and haptophytes, respectively. Compositions reflect the contributions of three different biomarkers to the sum of them (∑BDA), indicating the composition of phytoplankton community.

the eigenweightings of each mode for further clarification (Table 3).

In spring, Mode 1 describes the impact of the MZCC, which is the primary physical process affecting phytoplankton biomass. The high-weighted area in Mode 1 corresponds well to the high-value area of the biomass indicator (∑PB) in (Figs 6a and 7a). According to the correlation analysis, the MZCC has a significant enhancing effect on both diatom and dinoflagellate biomass, but has a moderately limiting effect on haptophytes (Table 3). In the southern TS, SCSWC dominates Mode 2 as a secondary influence, leading to the prevalence of haptophytes (Figs 4i, 6a and 7a). The warm and saline water carried by the SCSWC aligns with the growth requirements of haptophytes (Zhong et al., 2020). Consequently, the presence of SCSWC significantly enhances haptophyte biomass and regulates their population aggregation in the southern region (Table 3 and Fig. 9a). Due to the location of our observation station on the western side of the TS, it may be challenging to accurately assess the response of haptophytes to the Kuroshio-affected water. Nevertheless, previous studies have indicated higher haptophyte biomass in the Kuroshio water (Tao et al., 2012; Zhong et al., 2020). Mixing is the tertiary physical process in spring, and although its impact on biomass is not considered significant, it moderately limits the growth of haptophytes. This process mainly affects the Jiulong River Estuary and TWB (Fig. 6a), and is a result of the river transport process occurring on both the east and west sides of the TS. From the western and eastern regions, terrestrially-sourced materials are transported by currents from the Wuqiu and Penghu Channel towards the center of the TS, respectively (Tao et al., 2022). This transport process plays a role in regulating the community structure of phytoplankton to some extent, but it is relatively slight.

In summer, prevailing SW monsoon winds along the west coast of the TS form favorable upwelling conditions (Hu et al., 2015; Liu et al., 2019). Our EOF results reveal a distinct influence of upwelling during the summer season (Mode 1 in summer, primary process), and these upwellings are distributed in a patchy pattern in the eigenweighting plot (Fig. 6b), which also aligns with the upwelling area division in the TS during summer as reported by Liu et al. (2019). The most significant effect is observed in the upwelling region of the Minjiang River Estuary (Fig. 6b), which could be attributed to the overlap between upwelling and the river plume in this region. It is worth noting that our terrestrial biomarkers also show positive performance, and this overlapping state has been reported and discussed in previous studies (Gan et al., 2010; Hong et al., 2009, 2011b; Liu et al., 2019). In addition, the distribution of ΣPB in summer also corresponds well to the upwelling regions, suggesting that the biomass in summer is controlled by the upwelling process (Figs 6b and 8b). Indeed, numerous studies have suggested that diatoms can contribute a major portion of the phytoplankton biomass in upwelling water (Anabalón et al., 2016; Du and Peterson, 2018; Zhong et al., 2020). We found that coastal upwelling significantly

Table 3. Controlling factors in different seasons based on the correlations of phytoplankton biomarkers versus the specific physical process mode

Season	Physical process	Diatom-derived biomarker	Dinoflagellate-derived biomarker	Haptophyte-derived biomarker	∑PB
Spring	MZCC	++	++	−	++
	SCSWC			++	
	Mixing water			−	
Summer	Coastal upwelling	++	+		++
	Kuroshio invasion	+	++	+	++
	River plumes				
Autumn	Resuspension	−−	−−	−	−−
	MZCC				
	Residual upwelling		+		
Winter	MZCC		+	−	
	Mixing water	+	+	++	+
	Resuspension	−			−

Note: Correlation coefficients larger than |±0.6| is significantly enhance/limit (++/−−); larger than |±0.3| and less than |±0.6| are moderately enhance/limit (+/−); less than |±0.3| do not have a enhance/limit effect. For specific correlation coefficient values, see Table S1. ∑PB: biomass indicated by the sum of brassicasterol and dinosterol.

enhances diatom production, while it only moderately stimulates dinoflagellate production. It does not exhibit any notable promoting or inhibiting effect on haptophyte production (Table 3); therefore, in areas where coastal upwelling is prevalent, diatom communities have the absolute advantage towards growth in the phytoplankton community (Fig. 9b). The Kuroshio invasion mode is the secondary physical process mode in summer. It is noteworthy that this mode particularly affects the northeastern region of the study area which has significantly enhanced phytoplankton biomass (Table 3). This increase in biomass may be attributed to the intrusion of the deep-layer Kuroshio Current into the ECS shelf during summer. The deep-layer Kuroshio Branch water carries nutrient-rich bottom water, which can significantly impact ecosystems on the ECS shelf (Yang et al., 2017). Our findings indicate that all three major phytoplankton groups experience growth stimulation in Kuroshio water. However, dinoflagellates demonstrate a superior performance compared to the other two groups. The intrusion of Kuroshio water significantly enhances the growth of dinoflagellates, while the other two groups experience a moderate enhancement (Table 3 and Fig. 9b). One possible explanation is that dinoflagellates may possess the capability to modify their ecological niche in response to environmental changes, enabling them to adapt to warmer conditions (Irwin et al., 2015; Meng et al., 2018).

In autumn, the monsoon winds from the north start to strengthen, resulting in the invasion of the ZMCC into the strait. At the same time, the warm current in the SCS recedes (Li et al., 2006). In our study, phytoplankton growth was in a sluggish state, and most of the biomass was concentrated in the central to southern regions (Fig. 7c). This was somewhat similar to the observation by Li et al. (2006) that TS phytoplankton biomass during autumn was concentrated in the central and northern regions. Additionally, this biomass pattern is strongly associated with the resuspension mode in autumn (Figs 6c and 7c). The resuspension mode is the primary process in autumn, and its high turbidity characteristics often hinder the growth of all groups of phytoplankton and lead to low biomass (Table 3). Low biomass of phytoplankton caused by the light limitation from increased turbidity has been confirmed in many sea areas such as the ECS (Wu et al., 2016), the coastal waters surrounding Qatar (Arabian Gulf) (Quigg et al., 2013), and marginal ice zones (Fitch and Moore, 2007). On the contrary, areas with less obvious resuspension are areas where biomass is relatively high (Figs 6c and 7c). As the secondary physical process in autumn, although the MZCC can bring abundant nutrients, it did not significantly enhance biomass. It is worth mentioning that the tertiary physical mode—the river plume mode, has a moderate enhancing effect on dinoflagellate production (Table 3).

In winter, when the northeasterly winds become strong, the low-temperature, low-salinity and nutrient-rich MZCC on the western side of the TS can extend as far south as Dongshan Island (Zhong et al., 2020). The MZCC mode has become the primary physical mode during the winter period. However, even though its influence on phytoplankton biomass is significant, this influence is not noteworthy. It does not significantly enhance or limit diatom production, and only moderately limits haptophytes and a moderately enhances dinoflagellates (Table 3). This suggests that dinoflagellates can make a greater contribution to biomass in nearshore waters affected by coastal currents, which is consistent with findings by Zhong et al. (2020). Meanwhile, due to the greater influence of turbidity, the MZCC may inhibit the growth of phytoplankton to some extent, particularly in nearshore coastal areas (Fig. 8d). The secondary physical mode is the mixing mode, which mainly focuses on the center of the strait and generally has a moderate enhancement of biomass (Fig. 6d and Table 3). This mode has a positive promoting effect on all three phytoplankton groups, especially haptophytes (Table 3). Similar to autumn, the resuspension mode continues to be significant during winter. However, it should be noted that the resuspension effect in winter might be slightly less pronounced, which exerts only a moderate constraint on biomass. Once again, the high turbidity and light limitation caused by resuspension often leads to the inhibition of biomass (Lin et al., 2022). In general, the biomass of phytoplankton was still low in winter, mainly occurring in the coastal areas in the middle of the strait. The composition of the phytoplankton community is still dominated by diatoms (Fig. 9d).

4.3 *Ecological variation triggered by the effects of highly dynamic fronts and upwelling processes*

Based on the EOF analysis, we have clarified the coupled relationship between biological and physical processes in the TS at a seasonal scale (Table 3). In our study, we found that distinct physical systems have a high degree of variability between seasons. For example, there were some differences in upwelling processes between summer and autumn. During the summer,

coastal upwelling primarily impacted the northern region, particularly near the mouth of the Minjiang River. As autumn progressed, the upwelling area became more scattered and predominantly affected the southern part of the study area (Figs 6b and c). This suggests that the fluctuation in the intensity of the SW monsoon plays a significant role in influencing the formation, duration, and decline of upwelling patterns in the TS, consequently resulting in ecological variability. This seasonal observation may also be applicable to longer timescales. For instance, previous studies have indicated that coastal upwelling in the TS exhibits notable interannual variability that is a local response to El Niño Southern Oscillation (ENSO) events (Hong et al., 2009; Kuo and Ho, 2004; Shang et al., 2005). The upwelling was stronger in years when the southwesterly winds in the TS were intensified. The wind variations can be traced back to the anomaly of the East Asian Monsoon, which develops after the ENSO onset in the previous year (Hong et al., 2009). Furthermore, global warming often interacts with climate phenomena such as ENSO events and affects regional wind patterns, which could then affect the strength of upwelling (Doney et al., 2012; Zhong et al., 2020). In addition, the MZCC also exhibits significant variability between seasons, influenced by the intensity of the NE monsoon. Its impact area may extend from the north (spring) to the south (winter), and can even reach Dongshan Island during the peak of the monsoon (Figs 6a, c and d). On multi-year timescales, the MZCC is also modulated by the ENSO cycle (Hong et al., 2011b; Zhong et al., 2022). During El Niño years, the MZCC flows southward as far as Xiamen, and strong SST fronts are formed and run across the central TS, while the MZCC is present only near the coast of the western TS in La Niña years (Zhong et al., 2022). Thus, the physical processes in the TS may be dynamic and highly variable. To better comprehend the evolving patterns of these dynamic physical processes and further elucidate the coupling response mechanism between biological and physical processes, there is an urgent need for long-term, continuous, high-resolution field data.

5 Conclusions

Phytoplankton biomass and community structures in the TS are controlled by seasonal forcing, which is usually associated with the physio-chemical properties of the dominant water masses. Based on EOF analysis, we have defined six independent physical processes that have direct/indirect impacts on phytoplankton communities. (1) the MZCC intrusion has a promoting effect on diatom and dinoflagellate production but an inhibitory effect on haptophyte production, and is the primary physical process affecting phytoplankton productivity in the TS during spring. (2) The emergence of the SCSWC has led to an increase in the biomass of haptophytes, which is the primary process affecting the spatiotemporal variations of haptophyte biomass in the TS. (3) The invasion of Kuroshio water during summer significantly enhances the growth of dinoflagellates, while the other two species experience only a moderate enhancement. (4) Coastal upwelling significantly enhances diatom biomass, while it has a moderately stimulating effect on dinoflagellates. However, it does not exhibit any notable promoting or inhibiting effect on haptophytes. In addition, coastal upwelling is the primary physical process affecting phytoplankton biomass in the TS during summer. (5) In general, river plumes play a role in regulating the biomass and community structure of phytoplankton to some extent, but it is relatively slight in the TS. (6) Resuspension is the primary process during autumn and an important process during winter, and its ensuing high turbidity often hinders the growth of phytoplankton, leading to low biomass and significant limiting effects on almost all algal species. Overall, this study of phytoplankton biomarkers in the upper water column provides a comprehensive understanding of the physical forcings that control the spatiotemporal variability in phytoplankton biomass and community structure. The findings presented here also offer valuable insights into the utilization of biomarkers in sedimentary records.

Acknowledgements

We thank Prof. James T. Liu, Dominique Valdivia, Jay Lee, Rick Yang from Sun Yat-sen University in Taiwan for their valuable technical guidance on EOF analysis. We also extend our appreciation to Dr. Thomas M. Blattmann from ETH-Zürich for his assistance in polishing the language and providing numerous insightful suggestions. This study is also supported by the Cultivating Innovation Team Program of Third Institute of Oceanography, MNR.

References

Anabalón V, Morales C E, González H E, et al. 2016. Micro-phytoplankton community structure in the coastal upwelling zone off Concepción (central Chile): annual and inter-annual fluctuations in a highly dynamic environment. Progress in Oceanography, 149: 174–188, doi: 10.1016/j.pocean.2016.10.011

Archer D E, Eshel G, Winguth A, et al. 2000. Atmospheric pCO_2 sensitivity to the biological pump in the ocean. Global Biogeochemical Cycles, 14(4): 1219–1230, doi: 10.1029/1999GB001216

Barlow R, Lamont T, Gibberd M J, et al. 2017. Phytoplankton communities and acclimation in a cyclonic eddy in the southwest Indian Ocean. Deep-Sea Research Part I: Oceanographic Research Papers, 124: 18–30, doi: 10.1016/j.dsr.2017.03.013

Baumann K H, Andruleit H, Böckel B, et al. 2005. The significance of extant coccolithophores as indicators of ocean water masses, surface water temperature, and palaeoproductivity: a review. Palä ontologische Zeitschrift, 79(1): 93–112

Bi Rong, Chen Xi, Zhang Jing, et al. 2018. Water mass control on phytoplankton spatiotemporal variations in the northeastern East China Sea and the western Tsushima Strait revealed by lipid biomarkers. Journal of Geophysical Research: Biogeosciences, 123(4): 1318–1332, doi: 10.1002/2017JG004340

Bianchi T S, Canuel E A. 2011. Chemical Biomarkers in Aquatic Ecosystems. Princeton: Princeton University Press

Brassell S C, Eglinton G, Marlowe I T, et al. 1986. Molecular stratigraphy: a new tool for climatic assessment. Nature, 320(6058): 129–133, doi: 10.1038/320129a0

Burdige D J. 2005. Burial of terrestrial organic matter in marine sediments: a re-assessment. Global Biogeochemical Cycles, 19(4): GB4011

Bustillos-Guzmán J, Claustre H, Marty J C. 1995. Specific phytoplankton signatures and their relationship to hydrographic conditions in the coastal northwestern Mediterranean Sea. Marine Ecology Progress Series, 124: 247–258, doi: 10.3354/meps124247

Chen Ning, Song Changchun, Xu Xiaofeng, et al. 2021. Divergent impacts of atmospheric water demand on gross primary productivity in three typical ecosystems in China. Agricultural and Forest Meteorology, 307: 108527, doi: 10.1016/j.agrformet.2021.108527

Chen Chen-Tung Arthur, Wang Shulun, Chou Wenchen, et al. 2006. Carbonate chemistry and projected future changes in pH and $CaCO_3$ saturation state of the South China Sea. Marine Chemistry, 101(3–4): 277–305, doi: 10.1016/j.marchem.2006.01.007

Ding Yang, Bi Rong, Sachs J, et al. 2019. Lipid biomarker production by marine phytoplankton under different nutrient and temperature regimes. Organic Geochemistry, 131: 34–49, doi: 10.1016/j.orggeochem.2019.01.008

Ding Ling, Xing Lei, Zhao Meixun. 2010. Applications of biomarkers for reconstructing phytoplankton productivity and community

structure changes. Advances in Earth Science (in Chinese), 25(9): 981–989
Doney S C, Ruckelshaus M, Emmett Duffy J, et al. 2012. Climate change impacts on marine ecosystems. Annual Review of Marine Science, 4: 11–37, doi: 10.1146/annurev-marine-041911-111611
Dong Liang, Li Li, Wang Hui, et al. 2012. Phytoplankton distribution in surface water of western Pacific during winter, 2008: a study of molecular organic geochemistry. Marine Geology & Quaternary Geology (in Chinese), 32(1): 51–59
Du Xiaoqin, Liu James T. 2017. Particle dynamics of the surface, intermediate, and benthic nepheloid layers under contrasting conditions of summer monsoon and typhoon winds on the boundary between the Taiwan Strait and East China Sea. Progress in Oceanography, 156: 130–144, doi: 10.1016/j.pocean.2017.06.009
Du Xiuning, Peterson W T. 2018. Phytoplankton community structure in 2011–2013 compared to the extratropical warming event of 2014–2015. Geophysical Research Letters, 45(3): 1534–1540, doi: 10.1002/2017GL076199
Falkowski P G, Ziemann D, Kolber Z, et al. 1991. Role of eddy pumping in enhancing primary production in the ocean. Nature, 352(6330): 55–58, doi: 10.1038/352055a0
Fawcett S E, Ward B B. 2011. Phytoplankton succession and nitrogen utilization during the development of an upwelling bloom. Marine Ecology Progress Series, 428: 13–31, doi: 10.3354/meps09070
Field C B, Behrenfeld M J, Randerson J T, et al. 1998. Primary production of the biosphere: integrating terrestrial and oceanic components. Science, 281(5374): 237–240, doi: 10.1126/science.281.5374.237
Fitch D T, Moore J K. 2007. Wind speed influence on phytoplankton bloom dynamics in the Southern Ocean Marginal Ice Zone. Journal of Geophysical Research: Oceans, 112(C8): C08006
Gan Jianping, Li Li, Wang Dongxiao, et al. 2009. Interaction of a river plume with coastal upwelling in the northeastern South China Sea. Continental Shelf Research, 29(4): 728–740, doi: 10.1016/j.csr.2008.12.002
Gan Jianping, Lu Zhongming, Dai Minhan, et al. 2010. Biological response to intensified upwelling and to a river plume in the northeastern South China Sea: a modeling study. Journal of Geophysical Research: Oceans, 115(C9): C09001
Gong Gwo Ching, Wen Yun Ho, Wang Bowen, et al. 2003. Seasonal variation of chlorophyll *a* concentration, primary production and environmental conditions in the subtropical East China Sea. Deep-Sea Research Part II: Topical Studies in Oceanography, 50(6–7): 1219–1236, doi: 10.1016/S0967-0645(03)00019-5
Grasshoff K, Kremling K, Ehrhardt M. 1999. Methods of Seawater Analysis. 3rd ed. Weinheim: Wiley
Gutiérrez-Rodríguez A, Safi K, Fernández D, et al. 2020. Decoupling between phytoplankton growth and microzooplankton grazing enhances productivity in subantarctic waters on Campbell Plateau, southeast of New Zealand. Journal of Geophysical Research: Oceans, 125(2): e2019JC015550, doi: 10.1029/2019JC015550
Harada N, Shin K H, Murata A, et al. 2003. Characteristics of alkenones synthesized by a bloom of *emiliania huxleyi* in the Bering Sea. Geochimica et Cosmochimica Acta, 67(8): 1507–1519, doi: 10.1016/S0016-7037(02)01318-2
Hassler C S, Djajadikarta J R, Doblin M A, et al. 2011. Characterisation of water masses and phytoplankton nutrient limitation in the East Australian Current separation zone during spring 2008. Deep-Sea Research Part II: Topical Studies in Oceanography, 58(5): 664–677, doi: 10.1016/j.dsr2.2010.06.008
Hernandez M T, Mills R A, Pancost R D. 2008. Algal biomarkers in surface waters around the Crozet plateau. Organic Geochemistry, 39(8): 1051–1057, doi: 10.1016/j.orggeochem.2008.04.015
Hernandez-Sanchez M T, Venables H J, Mills R A, et al. 2010. Productivity variation around the Crozet Plateau: a naturally iron fertilised area of the Southern Ocean. Organic Geochemistry, 41(8): 767–778, doi: 10.1016/j.orggeochem.2010.05.014
Hong Huasheng, Chai Fei, Zhang Caiyun, et al. 2011a. An overview of physical and biogeochemical processes and ecosystem dynamics in the Taiwan Strait. Continental Shelf Research, 31(S6): S3–S12
Hong Huasheng, Liu Xin, Chiang Kuo Ping, et al. 2011b. The coupling of temporal and spatial variations of chlorophyll *a* concentration and the East Asian monsoons in the southern Taiwan Strait. Continental Shelf Research, 31(S6): S37–S47
Hong Huasheng, Zhang Caiyun, Shang Shaoling, et al. 2009. Interannual variability of summer coastal upwelling in the Taiwan Strait. Continental Shelf Research, 29(2): 479–484, doi: 10.1016/j.csr.2008.11.007
Hu Jianyu, Kawamura H, Hong Huasheng, et al. 2001. Hydrographic and satellite observations of summertime upwelling in the Taiwan Strait: a preliminary description. Terrestrial, Atmospheric and Oceanic Sciences, 12(2): 415–430
Hu Jianyu, Kawamura H, Li Chunyan, et al. 2010. Review on current and seawater volume transport through the Taiwan Strait. Journal of Oceanography, 66(5): 591–610, doi: 10.1007/s10872-010-0049-1
Hu Jun, Lan Wenlu, Huang Bangqin, et al. 2015. Low nutrient and high chlorophyll *a* coastal upwelling system—A case study in the southern Taiwan Strait. Estuarine, Coastal and Shelf Science, 166: 170–177
Huang Ting Hsuan, Chen Chen-Tung Arthur, Zhang Wenzhou, et al. 2015. Varying intensity of Kuroshio intrusion into Southeast Taiwan Strait during ENSO events. Continental Shelf Research, 103: 79–87, doi: 10.1016/j.csr.2015.04.021
Irwin A J, Finkel Z V, Müller-Karger F E, et al. 2015. Phytoplankton adapt to changing ocean environments. Proceedings of the National Academy of Sciences of the United States of America, 112(18): 5762–5766
Jan Sen, Wang Joe, Chern Chingsheng, et al. 2002. Seasonal variation of the circulation in the Taiwan Strait. Journal of Marine Systems, 35(3–4): 249–268, doi: 10.1016/S0924-7963(02)00130-6
Jeng Woei Lih, Huh Chih An. 2004. Lipids in suspended matter and sediments from the East China Sea Shelf. Organic Geochemistry, 35(5): 647–660, doi: 10.1016/j.orggeochem.2003.12.002
Jiao Nianzhi, Liang Yantao, Zhang Yongyu, et al. 2018. Carbon pools and fluxes in the China Seas and adjacent oceans. Science China: Earth Sciences, 61(11): 1535–1563, doi: 10.1007/s11430-018-9190-x
Jin Haiyan, Zhuang Yanpei, Li Hongliang, et al. 2017. Response of phytoplankton community to different water types in the western Arctic Ocean surface water based on pigment analysis in summer 2008. Acta Oceanologica Sinica, 36(8): 109–121, doi: 10.1007/s13131-017-1033-z
Kang Lee Kuo, Lu Hsing Ming, Sung Pei Ting, et al. 2016. The summer distribution of coccolithophores and its relationship to water masses in the East China Sea. Journal of Oceanography, 72(6): 883–893, doi: 10.1007/s10872-016-0385-x
Kannan N, Kim M, Hong S H, et al. 2012. Chemical tracers, sterol biomarkers and satellite imagery in the study of a river plume ecosystem in the Yellow Sea. Continental Shelf Research, 33: 29–36, doi: 10.1016/j.csr.2011.10.001
Kinkel H, Baumann K H, Čepek M. 2000. Coccolithophores in the equatorial Atlantic Ocean: response to seasonal and Late Quaternary surface water variability. Marine Micropaleontology, 39(1–4): 87–112, doi: 10.1016/S0377-8398(00)00016-5
Kuo Nan Jung, Ho Chung Ru. 2004. ENSO effect on the sea surface wind and sea surface temperature in the Taiwan Strait. Geophysical Research Letters, 31(13): L13309
Lan Kuo Wei, Lee Ming An, Zhang C I, et al. 2014. Effects of climate variability and climate change on the fishing conditions for grey mullet (*Mugil cephalus* L.) in the Taiwan Strait. Climatic Change, 126(1–2): 189–202, doi: 10.1007/s10584-014-1208-y
Latasa M, Scharek R, Vidal M, et al. 2010. Preferences of phytoplankton groups for waters of different trophic status in the northwestern Mediterranean Sea. Marine Ecology Progress Series, 407: 27–42, doi: 10.3354/meps08559
Lee K E, Lee S, Park Y, et al. 2014. Alkenone production in the East

Sea/Japan Sea. Continental Shelf Research, 74: 1–10, doi: 10.1016/j.csr.2013.12.003
Lee Jay, Liu James T, Lin Yu Shih, et al. 2023. The contrast in suspended particle dynamics at surface and near bottom on the river-dominated northern South China Sea shelf in summer: implication on physics and biogeochemistry coupling. Frontiers in Marine Science, 10: 1156915, doi: 10.3389/fmars.2023.1156915
Li Shaojing, Huang Jiaqi, Guo Donghui, et al. 2006. Study on ecology of marine plankton in Taiwan Strait, China. Journal of Xiamen University: Natural Science (in Chinese), 45(S2): 24–31
Li Li, Liu Jie, He Juan, et al. 2014. Factors affecting the abundance and community structure of the phytoplankton in northern South China Sea in the summer of 2008: a biomarker study. Chinese Science Bulletin, 59(10): 981–991, doi: 10.1007/s11434-013-0106-4
Li Yuhong, Zhao Meixun, Zhang Hailong, et al. 2012. Phytoplankton biomarkers in surface seawater from the northern South China Sea in summer 2009 and their potential as indicators of biomass/community structure. Journal of Tropical Oceanography (in Chinese), 31(4): 96–103
Lin Jijiang, Hu Rijun, Wang Ping, et al. 2022. Surface sediment resuspension and suspended sediment transportation mechanism in the waters around Miaodao Strait. Marine Geology & Quaternary Geology (in Chinese), 42(3): 9–24
Liu James T, Huang Bangqin, Chang Yi, et al. 2019. Three-dimensional coupling between size-fractionated chlorophyll-*a*, POC and physical processes in the Taiwan Strait in summer. Progress in Oceanography, 176: 102129, doi: 10.1016/j.pocean.2019.102129
Liu James T, Kao Shuh Ji, Huh Chih An, et al. 2013. Gravity flows associated with flood events and carbon burial: Taiwan as instructional source area. Annual Review of Marine Science, 5: 47–68, doi: 10.1146/annurev-marine-121211-172307
Meng A, Corre E, Probert I, et al. 2018. Analysis of the genomic basis of functional diversity in dinoflagellates using a transcriptome-based sequence similarity network. Molecular Ecology, 27(10): 2365–2380, doi: 10.1111/mec.14579
Mineeva N M. 2021. Long-term dynamics of photosynthetic pigments in plankton of a large plains reservoir. Biosystems Diversity, 29(1): 10–16, doi: 10.15421/012102
Nakanishi T, Yamamoto M, Irino T, et al. 2012. Distribution of glycerol dialkyl glycerol tetraethers, alkenones and polyunsaturated fatty acids in suspended particulate organic matter in the East China Sea. Journal of Oceanography, 68(6): 959–970, doi: 10.1007/s10872-012-0146-4
NOAA. 2021. Global Monitoring Laboratory—Carbon cycle greenhouse gases. Maryland: National Oceanic and Atmospheric Administration
Quigg A, Al-Ansi M, Al Din N N, et al. 2013. Phytoplankton along the coastal shelf of an oligotrophic hypersaline environment in a semi-enclosed marginal sea: Qatar (Arabian Gulf). Continental Shelf Research, 60: 1–16, doi: 10.1016/j.csr.2013.04.015
Resio D T, Hayden B P. 1975. Recent secular variations in mid-Atlantic winter extratropical storm climate. Journal of Applied Meteorology, 14(7): 1223–1234, doi: 10.1175/1520-0450(1975)014<1223:RSVIMA>2.0.CO;2
Ryan J P, McManus M A, Sullivan J M. 2010. Interacting physical, chemical and biological forcing of phytoplankton thin-layer variability in Monterey Bay, California. Continental Shelf Research, 30(1): 7–16, doi: 10.1016/j.csr.2009.10.017
Sarthou G, Timmermans K R, Blain S, et al. 2005. Growth physiology and fate of diatoms in the ocean: a review. Journal of Sea Research, 53(1–2): 25–42, doi: 10.1016/j.seares.2004.01.007
Scharek R, Tupas L M, Karl D M. 1999. Diatom fluxes to the deep sea in the oligotrophic North Pacific gyre at Station ALOHA. Marine Ecology Progress Series, 182: 55–67, doi: 10.3354/meps182055
Schubert C J, Villanueva J, Calvert S E, et al. 1998. Stable phytoplankton community structure in the Arabian Sea over the past 200 000 years. Nature, 394(6693): 563–566, doi: 10.1038/29047
Shang Shaoling, Zhang Caiyun, Hong Huasheng, et al. 2005. Hydrographic and biological changes in the Taiwan Strait during the 1997–1998 El Niño winter. Geophysical Research Letters, 32(11): L11601
Showstack R. 2013. Carbon dioxide tops 400 ppm at Mauna Loa, Hawaii. Eos, Transactions American Geophysical Union, 94(21): 192–192
Sicre M A, Tian R C, Saliot A. 1994. Distribution of sterols in the suspended particles of the Chang Jiang Estuary and adjacent East China Sea. Organic Geochemistry, 21(1): 1–10, doi: 10.1016/0146-6380(94)90083-3
Tang Danling, Kester D R, Ni I Hsun, et al. 2002. Upwelling in the Taiwan Strait during the summer monsoon detected by satellite and shipboard measurements. Remote Sensing of Environment, 83(3): 457–471, doi: 10.1016/S0034-4257(02)00062-7
Tang Danling, Ni I Hsun, Müller-Karger F E, et al. 2004. Monthly variation of pigment concentrations and seasonal winds in China's marginal seas. Hydrobiologia, 511(1–3): 1–15
Tao Shuqin, Liu James T, Wang Aijun, et al. 2022. Deciphering organic matter distribution by source-specific biomarkers in the shallow Taiwan Strait from a source-to-sink perspective. Frontiers in Marine Science, 9: 969461, doi: 10.3389/fmars.2022.969461
Tao Shuqin, Xing Lei, Luo Xiaofan, et al. 2012. Alkenone distribution in surface sediments of the southern Yellow Sea and implications for the $U^{K'}_{37}$ thermometer. Geo-Marine Letters, 32(1): 61–71, doi: 10.1007/s00367-011-0251-1
Tolosa I, Miquel J C, Gasser B, et al. 2008. Distribution of lipid biomarkers and carbon isotope fractionation in contrasting trophic environments of the South East Pacific. Biogeosciences, 5(3): 949–968, doi: 10.5194/bg-5-949-2008
Tseng Hsiao Chun, You Wan Lynn, Huang Wei, et al. 2020. Seasonal variations of marine environment and primary production in the Taiwan Strait. Frontiers in Marine Science, 7: 38, doi: 10.3389/fmars.2020.00038
Turner J T. 2015. Zooplankton fecal pellets, marine snow, phytodetritus and the ocean's biological pump. Progress in Oceanography, 130: 205–248, doi: 10.1016/j.pocean.2014.08.005
Wu Peng, Bi Rong, Duan Shanshan, et al. 2016. Spatiotemporal variations of phytoplankton in the East China Sea and the Yellow Sea revealed by lipid biomarkers. Journal of Geophysical Research: Biogeosciences, 121(1): 109–125, doi: 10.1002/2015JG003167
Wu Kai, Dai Minhan, Chen Junhui, et al. 2015. Dissolved organic carbon in the South China Sea and its exchange with the Western Pacific Ocean. Deep-Sea Research Part II: Topical Studies in Oceanography, 122: 41–51, doi: 10.1016/j.dsr2.2015.06.013
Xing Lei, Zhang Hailong, Yuan Zineng, et al. 2011. Terrestrial and marine biomarker estimates of organic matter sources and distributions in surface sediments from the East China Sea shelf. Continental Shelf Research, 31(10): 1106–1115, doi: 10.1016/j.csr.2011.04.003
Xu Qian, Sukigara C, Goes J I, et al. 2019. Interannual changes in summer phytoplankton community composition in relation to water mass variability in the East China Sea. Journal of Oceanography, 75(1): 61–79, doi: 10.1007/s10872-018-0484-y
Yamaguchi H, Ishizaka J, Siswanto E, et al. 2013. Seasonal and spring interannual variations in satellite-observed chlorophyll-*a* in the Yellow and East China Seas: new datasets with reduced interference from high concentration of resuspended sediment. Continental Shelf Research, 59: 1–9, doi: 10.1016/j.csr.2013.03.009
Yang Rick J, Liu James T, Su Chih Chieh, et al. 2021. Land-ocean interaction affected by the monsoon regime change in western Taiwan Strait. Frontiers in Marine Science, 8: 735242, doi: 10.3389/fmars.2021.735242
Yang Dezhou, Yin Baoshu, Hou Yijun, et al. 2017. Advance in research on Kuroshio intrusion and its ecological influence on the continental shelf of East China Sea. Oceanologia et Limnologia Sinica (in Chinese), 48(6): 1196–1207
Zhao Meixun, Mercer J L, Eglinton G, et al. 2006. Comparative molecular biomarker assessment of phytoplankton paleoproductivity for the last 160 kyr off Cap Blanc, NW Africa. Organic Geochemistry, 37(1): 72–97, doi: 10.1016/j.orggeochem.2005.

08.022
Zhao Bin, Yao Peng, Bianchi T S, et al. 2021. Controls on organic carbon burial in the eastern China marginal seas: a regional synthesis. Global Biogeochemical Cycles, 35(4): e2020GB006608, doi: 10.1029/2020GB006608
Zhong Yanping, Laws E A, Zhuang Jiafu, et al. 2022. Responses of phytoplankton communities driven by differences of source water intrusions in the El Niño and La Niña events in the Taiwan Strait during the early spring. Frontiers in Marine Science, 9: 997591, doi: 10.3389/fmars.2022.997591
Zhong Yanping, Liu Xin, Xiao Wupeng, et al. 2020. Phytoplankton community patterns in the Taiwan Strait match the characteristics of their realized niches. Progress in Oceanography, 186: 102366, doi: 10.1016/j.pocean.2020.102366

Supplementary information:

Fig. S1. Distribution of temperature (℃) in surface water of four seasons in the TS: spring (a), summer (b), autumn (c), and winter (d). The black lines on land represent rivers.

Fig. S2. Distribution of salinity in surface water of four seasons in the TS: spring (a), summer (b), autumn (c), and winter (d). The black lines on land represent rivers.

Fig. S3. Distribution of nutrients in surface water of four seasons in the TS during 2019-2020: nitrate (μmol/L, a–d), phosphate (μmol/L, e–h), and silicate (μmol/L, i–l). The black lines on land represent rivers.

Fig. S4. The results of linear regression analysis of three nutrient parameters plotted against each other in a scatter plot. The uppergraph depicts the correlation between nitrate and silicate, while the lower graph represents the correlation between phosphate andsilicate.

Table S1. Controlling factors in different seasons based on the correlations of phytoplankton biomarkers versus the specific physicalprocess mode.

The supplementary information is available online at https://doi.org/10.1007/s13131-024-2380-1and http://www.aosocean.com/. The supplementary information is published as submitted, without typesetting or editing. The responsibility for scientific accuracy and content remains entirely with the authors.